DEC 23 1946

ACR No. L4E10

NATIONAL ADVISORY COMMITTEE FOR AERONAUTICS

WARTIME REPORT

ORIGINALLY ISSUED
May 1944 as
Advance Confidential Report L4E10

ESTIMATION OF PRESSURES ON COCKPIT CANOPIES, GUN TURRETS, BLISTERS, AND SIMILAR PROTUBERANCES

By Ray H. Wright

Langley Memorial Aeronautical Laboratory
Langley Field, Va.

NACA

LANGLEY MEMORIAL AERONAUTICAL LABORATORY
Langley Field, Va.

WASHINGTON

NACA WARTIME REPORTS are reprints of papers originally issued to provide rapid distribution of advance research results to an authorized group requiring them for the war effort. They were previously held under a security status but are now unclassified. Some of these reports were not technically edited. All have been reproduced without change in order to expedite general distribution.

3 1176 01364 9539

NACA ACR No. L4E10

NATIONAL ADVISORY COMMITTEE FOR AERONAUTICS

ADVANCE CONFIDENTIAL REPORT

ESTIMATION OF PRESSURES ON COCKPIT CANOPIES, GUN TURRETS, BLISTERS, AND SIMILAR PROTUBERANCES

By Ray H. Wright

SUMMARY

Methods are described for estimating pressure distributions over protuberances such as cockpit canopies, gun turrets, blisters, scoops, and sighting domes. These methods are applied to the estimation of the pressure distributions over spherical-segment and faired gun turrets and over the protuberances on the Brewster SB2A-1 airplane. The effects of compressibility, interference, and flow separation are discussed. It is shown that, by a combination of experimental data with theoretical methods, limiting pressures for use in determining maximum loads can in many cases be satisfactorily estimated. Much systematic experimentation is needed, however, to improve the accuracy of estimation.

INTRODUCTION

The purpose of the present report is to describe methods by which pressures and hence loads on protuberances, such as cockpit canopies, gun turrets, blisters, scoops, and sighting domes, may be roughly estimated. In particular, the possibility of determining limiting values of the pressure coefficient - values which cannot be exceeded in practice - is demonstrated.

The investigation was initiated by a request from the Bureau of Aeronautics, Navy Department, for load data on gun turrets. No applicable experimental data were available and, as the NACA testing facilities were already committed to other investigations, it was decided to estimate the limiting loads.

Methods generally useful in the estimation of loads on protuberances are described in the present report. These methods are applied and, where possible, the

results are compared with experimental data. The methods are necessarily only approximate. Even if the potential flow could be exactly calculated, the actual flow would likely depart so widely from the calculated flow as to render the results invalid. The exercise of judgment, based on experience, and the use of experiment in evaluating the effects of boundary layer, separation, compressibility, interference, and departure of the shape from that for which pressures can be computed are necessary in order to arrive at useful results.

Although little opportunity for systematic experimentation is likely at present, the study presented herein is being applied to turret shapes on particular airplane models being investigated at LMAL with a view toward improving the methods of estimation of pressures.

SYMBOLS

p	pressure
V	velocity
ρ	mass density
q	dynamic pressure, free stream unless otherwise stated $\left(\frac{1}{2}\rho V^2\right)$
P	pressure coefficient $\left(\frac{p_l - p_o}{q}\right)$
M	Mach number, free stream unless otherwise stated
ΔV	velocity increment
$\Delta V/V_o$	velocity-increment coefficient
V/V_o	velocity coefficient $\left(1 + \frac{\Delta V}{V_o}\right)$
γ	ratio of specific heat at constant pressure to specific heat at constant volume $\left(\frac{c_p}{c_v}\right)$
x,y	Cartesian coordinates

[redacted]

Z, ζ complex variables

Subscripts:

1 incompressible or low speed

o in undisturbed stream

l local

Other symbols are introduced and defined as needed. Insofar as possible, the notations of the references are retained in the present report. For this reason, more than one quantity may be designated by the same symbol or one quantity may be designated by more than one symbol.

METHODS FOR CALCULATION OF VELOCITIES OVER PROTUBERANCES

Although the airplane with its canopy, turrets, blisters, and other protuberances is a complicated three-dimensional form about which even the potential flow cannot now be computed, an estimate of the pressures on the protuberances can be obtained. The airplane presents the general appearance of a wing, fuselage, and tail with the protuberances superposed. These protuberances are usually of small length relative to the length of the fuselage or to the chord of the wing and are very often quite thick in relation to their length. The loads over these protuberances therefore are assumed to be determined largely by the shapes of the protuberances and to be modified by the interference of the wing and fuselage. As an approximation that is usually valid unless the protuberance is located near the nose or in the wake of the body, the total velocity V is assumed to be equal to the sum of the velocity over the protuberance without interference and the induced velocity increment ΔV due to the interfering bodies or, in coefficient form,

$$\frac{V}{V_o} = \left(\frac{V}{V_o}\right)_{\text{protuberance alone}} + \left(\frac{\Delta V}{V_o}\right)_{\text{interference}} \qquad (1)$$

[redacted]

Methods of determining the velocity increment due to interference are given in the appendix of reference 1. In many cases, the interference is sufficiently small that it may be neglected.

It is convenient and sufficiently accurate to apply the compressibility correction to the pressure coefficient estimated for incompressible flow

$$P_i = 1 - \left(\frac{V_i}{V_o}\right)^2 \qquad (2)$$

where V_i/V_o is the value of equation (1) for incompressible flow. The pressure coefficient for compressible flow is then obtained from an approximation given by Prandtl in reference 2 as

$$P = \frac{P_i}{\sqrt{1 - M^2}} \qquad (3)$$

where M is the stream Mach number. An approximation that in specific instances has been found to describe experimental results more accurately than Prandtl's method has been given by von Kármán in reference 3 as

$$P = \frac{P_i}{\sqrt{1 - M^2} + \dfrac{M^2 P_i}{2\left(1 + \sqrt{1 - M^2}\right)}} \qquad (4)$$

Equation (3) is sufficiently accurate, however, for the estimations described herein.

The pressure distributions obtained up to this point apply in potential flow. The effects of departure from potential flow, which include development of the boundary layer on the surface forward of the protuberance, separation of the flow, which occurs regularly on the rear of blunt bodies, and interaction of these effects with compressibility must now be estimated. Although the boundary layer and the point and existence of separation might be calculated, at least for low speeds, by the methods of references 4 and 5 (with modification

[redacted]

of the momentum equation for the three-dimensional flow), no method is known for calculating the corresponding pressures nor is any theory available for estimating the compressibility interaction. From the meager experimental data available, these effects can be at least qualitatively estimated. (These data are presented and discussed in the section entitled "Applications.") In brief, the procedure is as follows:

(1) Estimate the velocity-coefficient distribution for incompressible potential flow over the protuberance shape

(2) Estimate the interference velocity coefficients for incompressible potential flow

(3) Add the coefficients obtained in steps (1) and (2) as in equation (1)

(4) By use of step (3), compute the pressure coefficients for incompressible flow (equation (2))

(5) Apply the compressibility correction (equation (3) or (4))

(6) Estimate the effects of departure from potential flow

In practice, as appears in the examples, some modification of this procedure may be necessary.

The rest of this section is concerned largely with the determination of the velocity distribution with potential flow over specific protuberance shapes without interference.

General Considerations

Protuberances often appear as bodies that are approximately half of symmetrical forms cut by an infinite plane as indicated in figure 1. The flow without the interference is then theoretically approximate to the corresponding half of that over the complete body. In many cases the half-body approaches the two-dimensional form (airfoil), for which the pressure distribution is always calculable; then, as the pressure changes are larger in the two-dimensional than in the three-dimensional case, it is conservative to consider the

[redacted]

flow two dimensional. In other cases the shapes may approximate simple three-dimensional forms, such as spheres and prolate or oblate spheroids for which the flow is known, and the corresponding pressure distributions may be assumed.

If the form of the body or half-body is such that the flow cannot be directly calculated, it may be approximated by various devices. If the shapes of the front and rear edges of a protuberance are different, inasmuch as the flow over one edge is often little affected by that over the other, it may be possible to compute the pressure distributions over front and rear edges separately and to join the distributions at the center.

In some cases a simple body, for which the flow in three dimensions can be calculated, may be modified by a two-dimensional method to approximate a given shape. Such a modification depends upon the assumption that a small local change in the radius of a body of revolution produces a local two-dimensional effect. As the radius r of the body of revolution becomes larger, this assumption becomes more nearly correct. For example, the pressures over the lip of an open engine cowling approach the pressures over an airfoil with the profile shape of the lip and with the same effective angle of attack. An example of an oblate spheroid modified to approach the shape of the Maxson turret on the Brewster S52A-1 airplane is given in the section entitled "Applications."

Two-Dimensional Shapes

Arbitrary forms.- The two-dimensional potential flow past symmetrical profiles that correspond to given half-bodies can be obtained by the method of Theodorsen and Garrick (reference 6). In many cases, however, less laborious methods suffice. The graphical method of Jones and Cohen (reference 7) is well suited to the computation of potential flow over bumps.

Forms for which potential flow is known.- In certain cases, the form of the protuberance approaches that of some two-dimensional profile for which the pressure distribution or corresponding velocity distribution is already known and can be applied without much further computation. Three such simple profiles are the infinitely long circular cylinder, the ellipse, and the

[redacted]

double-circular-arc profile. For the circular cylinder moving normal to its axis, the velocity distribution with potential flow is given by

$$V = 2V_o \sin \theta \tag{5}$$

where θ is the polar angle measured from the stream direction and V_o is the forward or stream velocity.

The velocity distribution about the elliptic cylinder moving parallel to its major axis is given by Zahm in reference 8 and may be expressed in the form

$$V = V_o \left(1 + \frac{b}{a}\right) \sqrt{\frac{1 - \left(\frac{x}{a}\right)^2}{1 - \left(\frac{x}{a}\right)^2 + \left(\frac{b}{a}\right)^2 \left(\frac{x}{a}\right)^2}} \tag{6}$$

where

a semimajor axis

b semiminor axis

x distance along major axis from center

The forward portion of a symmetrical airfoil shape with zero lift can often be approximated by an ellipse as in figure 1(c). If $x_{y_{max}}$ is the distance from the nose at which the maximum ordinate y_{max} occurs, the equivalent ellipse can usually be determined from

$$\frac{b}{a} = \frac{y_{max}}{x_{y_{max}}}$$

The velocity distribution over the forward portion of the airfoil may then be taken the same as that on the ellipse.

Another very useful shape is the double-circular-arc symmetrical airfoil, of which the upper and lower surface profiles are arcs of the same circle. The

[redacted]

conformal transformation into a circle is given by Glauert in reference 9. The velocity distributions, obtained by potential theory, are given for different thicknesses by the solid lines in figure 2.

Thin bodies by slope method.- A simple approximate two-dimensional method that has proved extremely useful has been included in a publication by Goldstein (reference 10). This method, which gives the velocity distribution as an integral function of the slope of a symmetrical profile, may be called the "slope method."

For the derivation of the slope method, the following two simplifying assumptions are necessary:

(1) The profile is sufficiently thin that the velocity is nowhere very different from stream velocity V_o

(2) The slope of the profile is everywhere small

These assumptions preclude the existence of stagnation points.

The symmetrical profile may be assumed to be represented by a distribution of sources dQ/dx along the chord c. The velocity increment $\Delta(\Delta V)$ at any point (x_o,y_o) on the profile (fig. 3) due to the source element $\frac{dQ}{dx}dx$ at x is

$$\Delta(\Delta V) = \frac{\frac{dQ}{dx}dx}{2\pi r} \tag{7}$$

Because the profile is thin, the velocity at (x_o,y_o) cannot be very different from the velocity at x_o; thus,

$$\Delta(\Delta V) \approx \frac{\frac{dQ}{dx}dx}{2\pi (x_o - x)} \tag{8}$$

[redacted]

The total induced velocity therefore is

$$\Delta V \approx \int_0^c \frac{\frac{dQ}{dx}\,dx}{2\pi\,(x_o - x)} \qquad (9)$$

For unit length of the profile, the cross section at x is $2y$ and, with $V \approx V_o$, the volume flow is approximately equal to $2V_o y$. The volume flow through any cross section, however, must be equal to the total output of the sources upstream and, therefore,

$$Q \approx 2V_o y$$

or

$$\frac{dQ}{dx} = 2V_o \frac{dy}{dx} \qquad (10)$$

With substitution of the value of dQ/dx from equation (10) in equation (9), the coefficient of the induced velocity becomes

$$\frac{\Delta V}{V_o} \approx \frac{1}{\pi}\int_0^c \frac{\frac{dy}{dx}\,dx}{x_o - x} \qquad (11)$$

The integrand in equation (11) can be expressed in trigonometric form but, for the present purposes, the algebraic expression is retained. The velocity coefficient is given by

$$\frac{V}{V_o} = 1 + \frac{\Delta V}{V_o} \qquad (12)$$

If the slope dy/dx is known as an algebraic function of x, the velocity distribution can usually be obtained without much trouble as a function of x_o. The integrand in equation (11) approaches infinity or becomes indeterminate at $x = x_o$, but the integral

[redacted]

is usually finite; the infinite positive and negative strips cancel. If the integral approaches infinity at a given point x_0, a finite integral that yields a velocity increment which approximately agrees with the actual flow can usually be obtained for a slightly different value of x_0.

The slope method is more useful than might be supposed from the restrictions imposed in the derivation. Although the results are not exact, they provide a reasonably good approximation even for relatively thick forms, especially over regions of the profile having small slope. The method is not applicable in the vicinity of a stagnation point or where the slope dy/dx is large. This difficulty may, however, be circumvented. Many protuberance shapes involve no very large values of dy/dx and require no stagnation point. If a stagnation point does occur, the velocity distribution over the rest of the profile at some distance from the nose may be approximated provided the rounded nose or tail, which involves infinite slope, is extended in a cusp or otherwise is slightly altered to prevent very large values of dy/dx.

A reasonably accurate velocity computation can be made if the slope method is applied not to the given profile but to the shape obtained as the amounts Δy by which the ordinates of the given profile exceed those of a similar profile, such as ellipse or Joukowski airfoil, for which the velocity distribution is known. The velocity increments are simply superposed; that is, the required velocity distribution is the sum of the velocity distribution on the similar profile and the increment ΔV found for the difference shape. Three-dimensional shapes may be slightly modified in the same way.

Given protuberance profile shapes can often be approximated by the juxtaposition of a series of arcs for which the slopes are given as relatively simple algebraic functions - for example, circular, elliptic, and parabolic arcs. The induced-velocity coefficient $\Delta V/V_0$ may then be obtained from equation (11) by direct integration. This procedure yields approximately correct velocity distributions even though the curvature at the junctions may be discontinuous. The slope should obviously be made continuous; that is, the arcs should have the same slope at the juncture.

[redacted]

A protuberance profile may have the approximate shape of a single simple arc, such as the circular arc, in which case the velocity distribution is easily calculated. Thus, in figure 4,

$$\frac{dy}{dx} = - \tan \theta$$

$$x = r \sin \theta$$

$$dx = r \cos \theta \, d\theta$$

and equation (11) becomes

$$\frac{\Delta V}{V_o} = \frac{1}{\pi} \int_{-\theta_1}^{\theta_1} \frac{\sin \theta \, d\theta}{\sin \theta - \sin \theta_o}$$

$$= \frac{1}{\pi} \int_{-\theta_1}^{\theta_1} d\theta + \sin \theta_o \int_{-\theta_1}^{\theta_1} \frac{d\theta}{\sin \theta - \sin \theta_o} \qquad (13a)$$

Integration and substitution of the limits give

$$\frac{\Delta V}{V_o} = \frac{1}{\pi} \left\{ 2\theta_1 + \tan \theta_o \left[\log_e \left(\frac{\sin \theta_o \tan \frac{\theta_1}{2} + \cos \theta_o - 1}{\sin \theta_o \tan \frac{\theta_1}{2} - \cos \theta_o - 1} \cdot \frac{\sin \theta_o \tan \frac{\theta_1}{2} - \cos \theta_o + 1}{\sin \theta_o \tan \frac{\theta_1}{2} + \cos \theta_o + 1} \right) \right] \right\} \qquad (13b)$$

for the velocity distribution as a function of θ_o.

From figure 4,

$$\theta_1 = \sin^{-1} \frac{c}{2r}$$

$$\theta_o = \sin^{-1} \frac{x_o}{r}$$

and

$$\left(\frac{c}{2}\right)^2 = r^2 - (r - h)^2$$

or

$$r = \frac{h^2 + \frac{c^2}{4}}{2h}$$

from which

$$\theta_1 = \sin^{-1} \frac{4\frac{h}{c}}{1 + 4\left(\frac{h}{c}\right)^2} \qquad (14)$$

$$\theta_o = \sin^{-1} \frac{8\frac{x_o}{c}\frac{h}{c}}{1 + 4\left(\frac{h}{c}\right)^2} \qquad (15)$$

Substitution of equations (14) and (15) in equation (13b) gives the induced-velocity coefficient $\Delta V/V_o$ as a function of the chord position x_o/c and of the thickness ratio $2\frac{h}{c}$, where x_o/c is measured from the center as shown. The velocity increments for circular-arc profiles ranging in thickness ratio from 0.1 to 0.5 are shown in figure 2, in which the results of the slope method are compared with the results of the accurate conformal-transformation method. In figure 2, x/c is measured from the end of the profile rather than from the

[redacted]

center. Up to a thickness ratio of 0.2, the slope method gives a fair approximation of the velocity distributions over circular arcs. As was to be expected, the error is greater in regions of greater slope. The velocities at the center of the profile, where the slope is zero, are approximately correct even for the 50-percent-thick profile.

Three-Dimensional Shapes

Methods available for the calculation of flows in three dimensions are less general than the corresponding two-dimensional methods because, except in the special case of the ellipsoid with three unequal axes, they apply only to bodies possessing axial symmetry, that is, to bodies of revolution. Many protuberances are approximately axially symmetrical, however, and the three-dimensional theory may prove useful in estimating velocity and corresponding pressure distributions in these cases.

The sphere.- The simplest body of revolution is the sphere, for which the velocity distribution is given by

$$\frac{V}{V_o} = 1.5 \sin \theta \tag{16}$$

where the angle θ is measured along any meridian starting from the stream or flight direction.

The oblate spheroid.- A body of revolution resembling a gun turret is the oblate spheroid obtained by revolving the ellipse about its minor axis. Motion in the direction of a major axis of the ellipse as shown in figure 5 corresponds to that of the gun turret. The potential is given by Lamb (reference 11) in terms of the elliptic-cylindrical coordinates ξ, μ, and ω. At the surface of the oblate spheroid, $\xi = \xi_o$ and ξ_o is given by

$$\xi_o = \frac{b}{a} \frac{1}{\sqrt{1 - \left(\frac{b}{a}\right)^2}} \tag{17}$$

where a and b are the semimajor and semiminor axes, respectively, of the corresponding ellipse. From the

[redacted]

potential, the velocity distributions at the surface relative to the body may be derived.

Around the rim in the YZ-plane (line 1, fig. 5)

$$\left(\frac{V}{V_o}\right)_{rim} = L \sin \omega \tag{18}$$

where

$$L = \frac{2}{\zeta_o^2 + 2 - \zeta_o\left(\zeta_o^2 + 1\right)\cot^{-1} \zeta_o} \tag{19}$$

and ω is the angle with the plane containing the direction of flow and the polar axis as shown in figure 5 and is related to the distance along the Y-axis measured from the center by

$$y/a = \cos \omega$$

The velocity over the top in the XY-plane (line 2, fig. 5) is

$$\left(\frac{V}{V_o}\right)_{\omega=o} = L\mu\left(\frac{\zeta_o^2 + 1}{\zeta_o^2 + \mu^2}\right)^{1/2} \tag{20}$$

where

$$\mu = \sqrt{1 - \left(\frac{y}{a}\right)^2}$$

The velocity across the meridian lying in the XZ-plane (line 3) is

$$\left(\frac{V}{V_o}\right)_{\omega=\pi/2} = L \tag{21}$$

which, for a given thickness ratio b/a, is constant;

[redacted]

that is, the velocity at the surface across the meridian perpendicular to the motion of an oblate spheroid moving normal to its polar axis is constant. Although velocity distributions along other lines on the surface may be obtained, those given by equations (18), (20), and (21) are of greatest interest and are most simply derived.

The prolate spheroid.- A related body, for which the velocity distribution is more easily obtained than for the oblate spheroid, is the prolate spheroid moving parallel to its polar axis. The velocity distribution at the surface along any meridian as given by Zahm (reference 8) may be expressed as

$$\frac{V}{V_o} = (1 + k_a)\sqrt{\frac{1 - \left(\frac{x}{a}\right)^2}{1 - \left(\frac{x}{a}\right)^2 + \left(\frac{b}{a}\right)^2\left(\frac{x}{a}\right)^2}} \qquad (22)$$

where

$$k_a = -\frac{\log_e \frac{1+e}{1-e} - 2e}{\log_e \frac{1+e}{1-e} - \frac{2e}{1-e^2}}$$

where the eccentricity

$$e = \sqrt{1 - \left(\frac{b}{a}\right)^2}$$

and a and b are the semimajor and semiminor axes of the corresponding ellipse. The equivalent prolate spheroid can be employed to approximate the forward portion of a body of revolution in exactly the same way in which the ellipse was used to approximate the forward portion of a symmetrical airfoil. (See fig. 1.) The velocity distribution over the forward portion of the body of revolution may then be considered the same as that over the corresponding portion of the equivalent prolate spheroid.

[redacted]

Body of revolution represented by axial source distribution.- The velocity distribution about a body of revolution with flow parallel to the axis can be obtained by the method of von Kármán (reference 12), provided the body can be represented by a distribution of sources and sinks along the axis. This method is useful for a very regular body for which the shape of the meridian profile can be given by only a few ordinates. If the meridian profile is irregular, the method is tedious and perhaps impossible. It is described in detail in reference 12.

Body of revolution represented by doublet distribution along axis normal to flow.- The circular cylinder projecting from a plane surface A-A (fig. 6) is considered a half-body of which the other half is shown by dashed lines. At the plane of symmetry A-A, the velocity must lie parallel to the plane and tangential to the surface of the cylinder. At other planes, cross velocities occur and reduce the peaks; the maximum velocity changes consequently occur at the plane A-A, except possibly over the sharp corners at the ends for which the velocity distributions cannot be computed. By a method described by von Kármán (reference 12), the part of the polar axis occupied by the cylinder is covered with a doublet of moment per unit length equal to that obtained if the cylinder were infinite in length. The ends of the cylinder corresponding to this mathematical device are rounded rather than plane as shown; the influence of the rounded ends on the velocity distribution at the plane A-A must be small, however, and the ends of actual gun turrets are more likely to be rounded than plane. The pressure distributions in planes parallel to the plane A-A generally are similar, but the peaks are lower as the end of the cylinder is approached except that, in the region of small radius of curvature near a blunt end, high peaks may occur.

The velocity at the surface of the cylinder in the plane A-A is

$$\frac{V}{V_0} = (1 + \cos \theta) \sin \phi \qquad (23)$$

where ϕ is the polar angle measured from the plane containing the flow direction and the polar axis, θ is

[redacted]

the angle shown in figure 6 for which

$$\cos\theta = \frac{l}{\sqrt{r^2 + l^2}}$$

r is the radius of the cylinder, and l is the length of its projection from the surface. An example for which r is not constant is treated later. The method is described in reference 12.

Body of revolution by method of Kaplan.- A method has recently been developed by Kaplan (reference 13) by which the potential flow about any body of revolution moving in the direction of its polar axis may be calculated to any desired degree of approximation. By this method, the flow is obtained with orthogonal curvilinear coordinates for which the surface of the body itself is a constant. The coordinate system, which is different for each body, is obtained by means of the conformal transformation

$$z = Z + c_1 + \frac{a_1}{Z} + \frac{a_2}{Z^2} + \frac{a_3}{Z^3} + \ldots \qquad (24)$$

which transforms the circles η = Constant and the radial lines ξ = Constant in the plane $Z = Re^{\eta}e^{-i\xi}$ into the corresponding orthogonal coordinate lines in the z-plane, where $\eta = 0$ is the meridian profile of the body of revolution. The potential is given as a series of terms involving the Legendre functions P_n and Q_n and the constants a_n appearing in the series in equation (24).

The derivation of the necessary functions has been extended in reference 13 only far enough to take account of the term a_3/Z^3 in equation (24). If additional terms are necessary to describe the meridian profile to a sufficient degree of approximation, the corresponding functions must be derived. The method of derivation is described in detail in reference 13. Fewer terms of equation (24) are required as the profile is more regular and more nearly approximates the ellipse. For irregular

bodies, additional terms are required and the labor necessary to calculate the flow is greatly increased. The practical utility of the method is therefore much greater for regular bodies - such as airship shapes, fuselages, or nacelles - than for irregular shapes. For such regular bodies, the labor required is not excessive.

Approximate thin body.- A thin-body method applicable to bodies of revolution and corresponding to the slope method in two dimensions has been suggested by Munk (reference 14, p. 269). An attempt to use this method indicated that, with usual fineness ratios (less than 10), the accuracy was insufficient for estimating induced velocities over protuberances.

Approximate body of revolution for use with method of Kaplan.- If the transformation (24) is known (it can always be obtained by the method given in reference 6) and if the given meridian profile can be sufficiently well approximated by the first three or four terms of this transformation, the flow about a body of revolution moving in the direction of the polar axis may be calculated by Kaplan's method with no more labor than is required by the thin-profile method. The potential flow thus calculated is the potential flow about the body that corresponds to the terms retained in equation (24). If the given body of revolution does not depart too greatly from an ellipse, the required transformation may be approximated by a method of superposition.

The series of equation (24) can be written in the form

$$z = x + iy$$

$$= Z + \frac{a^2}{Z} + c_1 - \frac{\epsilon_1 Ra}{Z} - \frac{\epsilon_2 R^2 a}{Z^2} - \frac{\epsilon_3 R^3 a}{Z^3} \cdots \qquad (25)$$

where

$$Z = Re^{-i\zeta}$$

$$\zeta = \xi + i\eta$$

$$R = (1 + \epsilon)a$$

[redacted]

and a is a constant depending on the size of the body. On the profile ($\eta = 0$), equation (25) becomes

$$x_o + iy_o = (1 + \epsilon)a(\cos\xi - i \sin\xi) + \frac{a}{1 + \epsilon}(\cos\xi + i \sin\xi)$$
$$+ c_1 - \epsilon_1 a(\cos \xi + i \sin\xi)$$
$$- \epsilon_2 a(\cos 2\xi + i \sin 2\xi)$$
$$- \epsilon_3 a(\cos 3\xi + i \sin 3\xi) \qquad (26)$$

The first two terms of equation (26) give the ellipse

$$\left.\begin{aligned} \frac{x}{a} &= \left(1 + \epsilon + \frac{1}{1 + \epsilon}\right)\cos \xi \\ \frac{y}{a} &= -\left(1 + \epsilon - \frac{1}{1 + \epsilon}\right)\sin \xi \end{aligned}\right\} \qquad (27)$$

and the remaining terms give

$$\left.\begin{aligned} \frac{\Delta x}{a} &= c_1 - \epsilon_1 \cos \xi - \epsilon_2 \cos 2\xi - \epsilon_3 \cos 3\xi \ldots \\ \frac{\Delta y}{a} &= - \epsilon_1 \sin \xi - \epsilon_2 \sin 2\xi - \epsilon_3 \sin 3\xi \ldots \end{aligned}\right\} \qquad (28)$$

The coefficients ϵ_1, ϵ_2, and ϵ_3 may be so determined as to yield a slight modification of the ellipse approximating a given meridian profile. For a small modification of the ordinates, the abscissa x/a is only slightly changed and, as an approximation, the required modification $\Delta y/a$ may therefore be determined at the values of x/a for the ellipse. The ellipse to be used as a basis for the approximation should be so

[redacted]

chosen that the required modification is as small as possible. The value of ϵ corresponding to a given thickness ratio B/A, where B is the minor axis and A the major axis, is obtained from equation (27). Thus,

$$t = \frac{B}{A} = \frac{\left(\frac{y}{a}\right)_{max}}{\left(\frac{x}{a}\right)_{max}}$$

$$= \frac{1 + \epsilon - \frac{1}{1 + \epsilon}}{1 + \epsilon + \frac{1}{1 + \epsilon}}$$

and solution for ϵ gives

$$\epsilon = \sqrt{\frac{1 + t}{1 - t}} - 1 \qquad (29)$$

An example will clarify the method.

In figure 7(a) is shown a meridian profile to be approximated. The ellipse with $\epsilon = 0.20$, also shown in figure 7, is determined to be a satisfactory basic profile for the approximation. The required modification of the ellipse is shown in figure 7(e). For convenience in this modification, the values of $-0.1 \sin \xi$, $-0.1 \sin 2\xi$, and $-0.1 \sin 3\xi$ are plotted against x/a as computed from equation (27). It is seen from figures 7(b) to 7(d) with equation (23) that ϵ_1 changes the thickness of the profile while the symmetry is retained, ϵ_2 produces an asymmetry forward and rearward, and ϵ_3 increases the ordinate at the ends while the center is depressed. Inasmuch as the main adjustment required is the introduction of asymmetry (fig. 7(e)), ϵ_2 must be given some value. It is seen that a value of $\epsilon_2 = 0.1$ accounts for a large part of the modification required. Further adjustment requires the elevation of both ends while the center remains unaffected.

[redacted]

If one-half the elevation is accomplished with ϵ_1 and one-half with ϵ_3, the desired modification is achieved. Because the required elevation $\Delta y/a$ is -0.05, the values of these coefficients are

$$\epsilon_1 = 0.025$$

$$\epsilon_3 = 0.025$$

The resulting coordinates from equations (27) and (28), shown as the first approximation in figure 7(a), are therefore

$$\frac{x}{a} = \left(1.2 + \frac{1}{1.2} - 0.025\right) \cos \xi - 0.1 \cos 2\xi - 0.025 \cos 3\xi$$

$$\frac{y}{a} = -\left(1.2 - \frac{1}{1.2} + 0.025\right) \sin \xi - 0.1 \sin 2\xi - 0.025 \sin 3\xi$$

The failure of the first approximation near the nose of the given profile is due largely to the reduction in x/a produced by ϵ_2. It is further evident that the forward part of the profile is more nearly approximated if the value of ϵ_2 is reduced from 0.10 to 0.07 and if the effect of ϵ_2 in reducing the value of x/a at the nose is neutralized by giving c_1 the value 0.07a. The resulting profile, which is a satisfactory approximation to the given profile, is shown as the second approximation in figure 7(a). A still better approximation is obtained if the value of c_1 is increased to 0.10a. The whole forward part of the given profile is then very closely approximated, and substitution of the values

$$\epsilon = 0.20 \qquad \epsilon_2 = 0.07$$

$$\epsilon_1 = \epsilon_3 = 0.025 \qquad c_1 = 0.10a$$

[redacted]

in equation (25) gives the required transformation

$$z = Z + 0.10a + \frac{0.97a^2}{Z} - \frac{0.1008a^3}{Z^2} - \frac{0.0432a^4}{Z^3}$$

from which the flow may be calculated without great difficulty by the method of reference 13.

Although the approximate method yields the potential flow about a shape somewhat different from the given profile, it is considered quite satisfactory for use in estimating loads. The approximate shape is likely to show slight bumps where none occur on the given profile, but the resulting pressure distribution is conservative in that it shows larger pressure variations than would be obtained for a more regular profile. On account of manufacturing irregularities, this conservatism may be desirable. Over the rear of a body, moreover, the actual flow always departs more or less from the potential flow, and little loss in accuracy may therefore be expected from any small failure of the approximation in that region. The method here employed should not be assumed the same as a simple harmonic analysis.

Corresponding bodies in two- and three-dimensional flows.- If the velocity distribution about a two-dimensional shape is known, a rough estimation of the velocity distribution about the body of revolution of which it is the meridian profile may be obtained from the ratio of velocities in three-dimensional flow to those in two-dimensional flow about corresponding bodies. The velocity distributions about the corresponding bodies - elliptical cylinders and prolate spheroids with motion parallel to the major axes - have been calculated by equations (6) and (22), respectively, and have been plotted for comparison in figure 8(a). Similarly, in figure 8(b), the velocity distributions obtained for approximately circular-arc bodies of revolution by the method of Kaplan are compared with the velocity distributions about the corresponding two-dimensional shapes. In figure 8, x is the distance from the nose of the body and l is its length.

Division of equation (22) by equation (6) gives for the ellipse and prolate spheroid

[redacted]

$$\frac{V_{3D}}{V_{2D}} = \frac{1 + k_a}{1 + \frac{b}{a}} \qquad (30)$$

where 3D indicates three-dimensional flow and 2D two-dimensional flow about corresponding bodies. Inasmuch as k_a is a function of the thickness ratio b/a of the corresponding ellipse, equation (30) shows that the velocity distribution about a prolate spheroid is a constant times the velocity distribution about the ellipse which is its meridian profile. The constant $\frac{V_{3D}}{V_{2D}}$ given by equation (30) is plotted in figure 9 as a function of the thickness ratio d/l. This relation suggests the possibility of using the corresponding two-dimensional shape to design a body of revolution similar to the prolate spheroid with a given velocity distribution.

The velocity ratio $\frac{V_{3D}}{V_{2D}}$ is not generally constant along the length, however, as may be seen from figure 8(b). In particular, the velocity over the tail of a three-dimensional body departs less from stream velocity than the velocity over the tail of the corresponding airfoil; the ratio $\frac{V_{3D}}{V_{2D}}$ therefore increases and exceeds unity as the trailing edge is approached. It is nevertheless reasonable to suppose that figure 9 could be used to estimate the velocities on bodies of revolution over the parts of the meridian profile that are roughly elliptical in shape. The following methods are suggested as alternatives:

(1) Fit an equivalent ellipse to the profile as in figure 1. With the thickness ratio of this ellipse, find the corresponding velocity ratio $\frac{V_{3D}}{V_{2D}}$ from figure 9.

[redacted]

(2) Assume that the corresponding ellipse is the one which has the same peak velocity as occurs on the profile. From equation (6), the corresponding thickness ratio d/l or b/a then is

$$t = \frac{b}{a} = \frac{V_{max}}{V_o} - 1 \qquad (31)$$

which with figure 9 gives the velocity ratio $\frac{V_{3D}}{V_{2D}}$.

As a test of the method, the velocity ratios $\frac{V_{3D}}{V_{2D}}$, which were constant along the length for the elliptical profiles but generally variable, were computed for several pairs of corresponding shapes. The variation along the length l is given in figure 10, in which the values of $\frac{V_{3D}}{V_{2D}}$ for the equivalent ellipses obtained by method (1) are shown for comparison. Method (2) would give quite similar values. For bodies of revolution with meridian profiles roughly similar to those for which the values of $\frac{V_{3D}}{V_{2D}}$ are known, these values may be used to obtain velocity estimates more nearly correct than can be obtained by use of the elliptical profiles alone. Relations similar to equation (30) can also be obtained for the oblate spheroid, but their application is less general than for the elongated bodies.

The ellipsoid with three unequal axes.- A protuberance shape not possessing axial symmetry - a flattened blister, for instance - may be approximated by an ellipsoid with three unequal axes. The necessary elliptical coordinates and the potential are given and explained in reference 14 on pages 293-302. The mathematical complexity is such that, in many cases, a less accurate approximation by means of the simpler body of revolution is preferred.

[redacted]

Estimation by Comparison

Comparison of the shape for which pressures are required with a somewhat similar shape for which the pressure distribution has been experimentally determined should prove very satisfactory if sufficiently extensive systematic experimentation had been completed; for the most part, however, only scattered data are available.

The only existing systematic investigation of pressure distributions over protuberances at high speeds is that for windshields and cockpit canopies given in reference 1. If a given shape approximates one of the shapes tested, the corresponding pressure distribution may be assumed. If a shape lies between two of those tested, its pressure distribution may also be assumed to lie between the two measured, provided no critical change in flow occurs - for example, separation or compressibility burble. If the canopy has no tail of its own but is faired directly into the fuselage (as in the case of the P-40 airplane), the pressure distribution over the forward part may be assumed independent of that over the tail and may be faired into that for the fuselage. In comparing canopies, the angle between the nose section and the hood is assumed an important variable because, for the small radii of curvature often found at the juncture between these two sections, the theoretical pressures, which are large negatively, are not attained; it therefore seems reasonable to suppose that the peak negative pressure coefficients are determined largely by the angle through which the stream must turn. These assumptions have not been thoroughly and systematically tested but, when applied to the estimation of the pressure distribution about the cockpit canopy of the P-40D airplane, gave results in substantial agreement with measurements subsequently obtained in the NACA 8-foot high-speed tunnel (unpublished).

The results of experiment may also be used to estimate the difference in pressure distributions between nearly similar bodies when the theoretical pressure distribution can be calculated for one of the bodies. Few data suitable for this purpose are available, however.

[redacted]

Experimental data used for comparison may include interference and compressibility effects; in this case, the difference in these effects must be estimated and a suitable adjustment applied.

APPLICATIONS

In this section of the present report, certain of the methods described in the preceding section are applied to the estimation of pressures over various protuberances, for some of which experimental pressure distributions are available for comparison. These and other experimental data are analyzed to determine how the methods should be applied and what modifications and adjustments are required to bring the estimated pressures into agreement with the experimental values.

Examples

Martin turret.- Complete low-speed pressure-distribution data for the Martin turret on a model of the North American B-25 fuselage are given in reference 15. The location of this turret on the fuselage is shown in figure 11(a). The pressure distributions are compared in figure 12 with the calculated values for the sphere and for the oblate spheroid with thickness ratio $b/a = 0.67$.

The theoretical estimation of the velocity distribution about this turret is particularly simple. The shape is that of a body of revolution almost elliptical in cross section and may therefore be represented by an oblate spheroid moving normal to its polar axis. The formulas for the velocity distribution over the top of the body in the direction of motion, across the top of the body in a plane perpendicular to the direction of motion, and around the rim of such a body are given in the section entitled "Methods." The interference from the fuselage should be small and, except for boundary layer and separation effects, the agreement between estimated and measured values should therefore be good. Figure 12 shows that the estimated negative pressure peak, in particular, is almost exactly the same as the value obtained from the measured pressures. Over the top of the turret in a plane perpendicular to the direction of motion, the theory indicates a constant pressure

[redacted]

and the measured values show almost constant pressure. Failure to reach stagnation pressure in front of the turret is due to the boundary layer developed over the fuselage; behind the turret, where the pressure coefficient approaches zero, stagnation pressure is not attained owing to separation.

Inasmuch as the pressures were measured at low speeds, no allowance has been made for compressibility effects. A rough estimation could be obtained by multiplying all pressure coefficients P by the factor

$$\frac{1}{\sqrt{1 - M^2}}$$

Turret A.- The two locations of turret A on the fuselage are shown in figure 11(b). Its shape and dimensions are given in figure 13. Pressure measurements on this turret are given in reference 16 and are plotted for comparison with estimated values in figure 14. Turret A is a spherical segment in form and is large compared with the fuselage, having only slightly smaller radius than the fuselage radius. About a third of the radius is projected above the fuselage. The turret is located back on the fuselage where the interference cannot be large. In consideration of this geometrical configuration, it is estimated that the pressure peaks cannot be greater in absolute value than would occur on the sphere and that, because of the interference of the fuselage and the development of the boundary layer along its surface, the peaks are probably lower. The change with Mach number up to $M = 0.70$ is assumed insufficient to cause the pressure coefficients to exceed in absolute value those calculated for the sphere by the potential theory. The theoretical pressure distribution for the sphere, as obtained from equation (16) with equation (2), is shown as the solid line in figure 14.

A velocity distribution of approximately the correct shape but with peaks higher than actually occur is obtained by applying the two-dimensional theory to the circular arcs over the top and side of the turret. The distribution of induced velocities, from which the pressure distribution is calculated by equations (2) and (12), can be obtained by interpolation for the proper thickness in figure 2. In this case, the velocity increments corresponding to the more accurate method of

[redacted]

conformal transformation from a circle are used. The pressure distributions obtained by this method for the 45-percent-thick circular arc on the top and for the approximately 27-percent-thick circular arc on the side are shown in figure 14.

The pressure on the rear of the body departs from the estimated values but, without the experimental data shown, the limits could hardly be fixed more closely than -0.45 for the circular cylinder (from unpublished data obtained in the NACA 8-foot high-speed tunnel) and 0.16 for the sphere (reference 17); however, a value close to zero would seem likely.

Turret B.- Turret B is described in reference 16. Its location on the fuselage is shown in figure 11(c) and the shape and dimensions are given in figure 15. A pressure distribution over the central profile (line 1, fig. 15), with peaks larger than are expected in practice, may be computed by the two-dimensional slope method. The integral indicated in equation (11) is made up of three parts, designated integrals I, II, and III, that correspond to the three divisions of the profile shown in figure 16. The integral I extending from $x = 0$ to $x = 2.88$ inches is obtained from equation (13) with the upper limit equal to 0 and the lower limit equal to θ_1. Integration and substitution of limits give

[redacted]

$$I = \frac{1}{\pi}\left\{-\theta_1 + \frac{\sin\theta_{o_1}}{1 - \sin^2\theta_{o_1}}\left[\log_e\left(\frac{\dfrac{1 - \sqrt{1 - \sin^2\theta_{o_1}}}{1 + \sqrt{1 - \sin^2\theta_{o_1}}}}{\dfrac{\sin\theta_{o_1}\tan\dfrac{\theta_1}{2} - 1 + \sqrt{1 - \sin^2\theta_{o_1}}}{\sin\theta_{o_1}\tan\dfrac{\theta_1}{2} - 1 - \sqrt{1 - \sin^2\theta_{o_1}}}}\right)\right]\right\}$$

where

$$\theta_1 = \sin^{-1}\frac{-2.88}{3.6}$$

$$\sin\theta_{o_1} = \frac{x - 2.88}{3.6}$$

For the values of x greater than 6.48 inches, $\sin\theta_{o_1}$ as here defined becomes greater than unity and integration gives I(a) instead of I, where

$$I(a) = \frac{1}{\pi}\left\{-\theta_1 + \frac{2\sin\theta_{o_1}}{\sqrt{\sin^2\theta_{o_1} - 1}}\left[\tan^{-1}\left(\frac{1}{\sqrt{\sin^2\theta_{o_1} - 1}}\right) - \tan^{-1}\left(\frac{1 - \sin\theta_{o_1}\tan\dfrac{\theta_1}{2}}{\sqrt{\sin^2\theta_{o_1} - 1}}\right)\right]\right\}$$

For the part of the profile lying between $x = 2.88$ inches and $x = 4.79$ inches, the appropriate integral II is obtained with the upper and lower limits in equation (13) equal to θ_2 and 0, respectively. Integration gives

$$II = \frac{1}{\pi}\left\{\theta_2 + \frac{\sin\theta_{o_2}}{\sqrt{1-\sin^2\theta_{o_2}}}\left[\log_e\left(\frac{\sin\theta_{o_2}\tan\frac{\theta_2}{2} - 1 + \sqrt{1-\sin^2\theta_{o_2}}}{\sin\theta_{o_2}\tan\frac{\theta_2}{2} - 1 - \sqrt{1-\sin^2\theta_{o_2}}}\,\frac{1-\sqrt{1-\sin^2\theta_{o_2}}}{1+\sqrt{1-\sin^2\theta_{o_2}}}\right)\right]\right\}$$

where

$$\theta_2 = \sin^{-1}\frac{1.91}{6}$$

$$\sin\theta_{o_2} = \frac{x - 2.88}{6}$$

The integral III from $x = 4.79$ inches to $x = 8.16$ inches as obtained from equation (11) with upper and lower limits of 8.16 and 4.79, respectively, and with $dy/dx = -0.3349$ is

$$III = \frac{-0.3349}{\pi} \log_e \frac{x - 4.79}{x - 8.16}$$

Then, for $x < 6.48$ inches,

$$\frac{\Delta V}{V_o} = I + II + III$$

and, for $x > 6.48$ inches,

$$\frac{\Delta V}{V_o} = I(a) + II + III$$

Calculated values have been converted to pressure coefficients, and the resulting distribution has been plotted as the solid line in figure 16. The coefficients then obtained are considered limiting values and are assumed sufficiently high in absolute value to allow for compressibility effects up to a Mach number of 0.70 and remain conservative.

From the calculated two-dimensional velocity distribution, the velocities about the corresponding body of revolution were estimated by the ratio of velocities in three-dimensional flow to those in two-dimensional flow as given for ellipses and prolate spheroids in figure 9. The corresponding pressure coefficients are shown as the dashed curve in figure 16. The shape of this turret is between the two-dimensional shape and the body of revolution and, consequently, the measured pressures lie between the estimated values for the profile and the values estimated for the body of revolution.

Cockpit canopy and gun turret on Brewster SB2A-1 airplane.- The shapes and locations of the cockpit canopy and gun turrets on the fuselage of the Brewster SB2A-1 airplane are shown in figure 17. Two alternative gun turrets have been suggested for this airplane. The top

[redacted]

shape of the Maxson turret approximates an oblate spheroid moving normal to the polar axis. The other turret is spherical in shape. The theoretical velocity distributions are computed first for the turret shapes alone without interference. The meridian profile of the Maxson turret is shown with pertinent dimensions in figure 18. Inasmuch as the shape is symmetrical, the pressure distribution is symmetrical from front to back and only one-half the half profile need be considered. The axes of figure 18 are arranged to correspond with those of figure 5. The turret profile is seen to be only slightly different from the ellipse with thickness ratio $b/a = 0.67$. The difference is shown as the short-dash line plotted along the y-axis. This difference can be approximated by a circular arc; and the turret profile shape thus can be more nearly approximated by adding to the ellipse in the region indicated the half thickness of the double circular arc of thickness ratio $t = 0.14$. The corresponding velocity ratio V/V_o is obtained by directly superposing the increments $\Delta V/V_o$, as found for the circular arc by interpolation in figure 2, on the values $\left(\frac{V}{V_o}\right)_{\omega=0}$ over the elliptical profile of the oblate spheroid. With $b/a = 0.67$, equation (17) gives $\zeta_o = 0.91$ and the velocity ratio over the elliptical section in the xy-plane is given by equation (20) for values of μ. The computation form is indicated in the following table:

μ	y/a	V/V_o for oblate spheroid	$\Delta V/V_o$ for 14-percent circular arc	V/V_o	$P = 1 - \left(\frac{V}{V_o}\right)^2$
0	±1.00	0	0	0	1.00
.20	±.98	.40	0	.40	.84
.40	±.92	.75	.05	.80	.36
.60	±.80	1.03	.14	1.17	-.37
.70	±.71	1.14	.18	1.32	-.74
.80	±.60	1.24	.15	1.39	-.93
.90	±.44	1.32	.06	1.38	-.90
.95	±.31	1.35	0	1.35	-.82
1.00	0	1.39	0	1.39	-.93

[redacted]

The velocity increments $\Delta V/V_o$ obtained by the two-dimensional method are likely to be somewhat large, and some small adjustment in the corresponding pressure coefficients must therefore be made. The pressure coefficients with these and other adjustments to be discussed later are plotted along the turret (line 1, fig. 19).

Around the circular rim of the turret, velocities somewhat higher than those about the rim of the oblate spheroid may be expected because of the departure of the turret from the true spheroidal shape and because of interference from the cylindrical sides of the turret extending down onto the fuselage. For use in the estimation, the velocity around the rim of the oblate spheroid is computed. With $\zeta_o = 0.91$, the velocity distribution $(V/V_o)_{rim}$ is obtained from equation (18) as a function of ω and is shown in the following table:

ω (deg)	$y/a = \cos\omega$	V/V_o	$P = 1 - \left(\frac{V}{V_o}\right)^2$
0	1.00	0	1.00
10	.98	.24	.94
20	.94	.47	.78
30	.87	.69	.52
40	.77	.89	.21
50	.64	1.06	-.12
60	.50	1.20	-.44
70	.34	1.30	-.69
80	.17	1.37	-.88
90	0	1.39	-.93

Again because of symmetry, this pressure distribution holds for negative values of y/a, that is, for ω between 90° and 180°.

For the spherical turret, shown in profile in figure 20, the theoretical velocity distribution over the meridian lying in the plane with the forward velocity was calculated from equation (16), and the pressure coefficients were obtained by equation (2). The values of y/a are obtained from $y/a = \cos\theta$, where again y is taken in the direction of motion.

[redacted]

For the cockpit canopy, the pressures over the nose and the general pressure distribution forward of station 121 (figs. 17, 19, and 20) were estimated from the data for the 8-4-5 windshield given in figure 22 of reference 1. The angle between the nose piece and the hood was 49° for the SB2A-1 windshield as compared with 48° for the 8-4-5 windshield; otherwise, the two windshields appeared similar. The data for a Mach number of about 0.70 were used, but the negative pressure peak was elevated slightly to allow for conservatism in regard to the somewhat sharper nose angle of the SB2A-1 windshield. The use of this pressure distribution involves the assumption that the difference between wing and fuselage interference in the two cases (airplane and model tested) is negligible. This assumption is reasonable because the wing and fuselage cannot differ greatly in the two cases and because the interference velocities are relatively small.

The bump in the pressure-distribution curve about station 49 is intended to represent the slight discontinuity at the rear of the sliding hatch cover. The dimensional data available do not permit the exact determination of the shape of the offset and, even if the shape were known, the calculated pressure distribution would be of questionable accuracy. The magnitude of the bump above the general pressure distribution was taken instead from the results of tests of a cockpit canopy similar to that of the SB2A-1 airplane.

The theoretical pressure distributions for the turret shapes are modified by interference, for which certain assumptions must be made. The turret is too close to the canopy and too large in relation to it for a ready estimate to be made of the effect of the canopy on the turret pressures; because the canopy is situated entirely ahead of the turret, however, the assumption can safely be made that the only effect of the canopy is to lower the velocities over the turret. The shape of the fuselage in the region of the turret is such that the induced velocities must be small and in addition it may be assumed that, because the wing is ahead of and not very close to the turret, the induced velocities due to the wing tend to be canceled by the induced velocities from the canopy. That these assumptions are reasonable is indicated by figure 22 of reference 1, in which the pressure coefficients behind the windshield with the tail and in the presence of wing and fuselage approach zero. If the canopy of the SB2A-1 airplane were faired out with a similar tail in the rear, moreover, the turret

would appear very similar to the half-sphere or half-spheroid on the tail. The flow over the part of the gun turret not thereby covered should be affected only slightly by extending the canopy straight back to the turret. The pressures over the top (line 1, figs. 19 and 20) have accordingly been taken as those over the modified spheroid and sphere, respectively, for which the theoretical distributions are given in the first part of this section.

Over the section indicated by line 3 in figures 17, 19, and 20, either turret contour is characterized by a circular-arc profile of about 50-percent thickness ratio superposed on the surface of the fuselage. Figure 2 gives the velocity distribution, which may be used with equation (2) to calculate the pressure distribution.

Over the rim (line 2, figs. 17, 19, and 20), the velocities must lie somewhere between those over the side (line 3) and those over the top (line 1). They are therefore taken to lie between the theoretical velocities over the rim of the oblate spheroid and those estimated for line 3, and the peak is assumed to be about the same as the theoretical peak for the sphere. The resulting curve is quite similar to that for the sphere and is taken to be the same for both turrets.

The pressures at line 4 must be determined largely by guess, because the contour itself is only slightly disturbed by the presence of the gun turret. The disturbance at line 3 must influence the velocities, however, and it therefore seemed reasonable to assume induced velocities one-half those at line 3. The corresponding pressure coefficients have been so calculated.

Behind the turret, because of separation, complete pressure recovery as indicated by the theoretical distributions is not attained. The pressure recovery shown in figures 19 and 20 is based on the tests of reference 15. The pressures on the rear of the circular cylinder and on the rear of the sphere are shown for comparison in figures 19 and 20 and are considered limiting values for low and moderate Mach numbers.

No adjustment of the pressure peaks has been made for the effect of compressibility because, for such blunt bodies, at least up to a Mach number of 0.70, the

[redacted]

conservatism of the methods used is assumed sufficient to cover the changes. Compressibility may, however, cause the separation point to move forward and thus lower the negative peaks and decrease the pressure behind the turrets. The negative pressure peaks therefore may be broadened backward, and some account of this effect has been taken in broadening the peaks in figures 19 and 20. In no case, however, at least up to a Mach number of 0.70, can the pressure on the rear of the turret decrease below the negative pressure peak that would be obtained in potential flow at the same Mach number. The negative pressure peak in figures 19 and 20 is thus indicated as the limit of the pressure on the rear of the turrets.

The development of the boundary layer over the canopy ahead of the turret and separation in the rear tend to prevent either positive or negative peaks in the pressure distribution from being as great as predicted; in this respect, the estimation is therefore conservative.

Average values of pressures obtained over the gun turret of the Brewster XSB2A-1 airplane in flight at speeds below 225 miles per hour (unpublished) are presented for comparison in figure 19. For obtaining loads, the estimation compares satisfactorily with the measured values though, for the top of the turret, it appears to be unconservative. From the data available, however, the turret on the XSB2A-1 airplane appears to project higher above the canopy than was assumed in the estimations and larger pressure peaks might therefore be expected. The irregularities in the measured pressure distribution may be caused by the ribs and other irregularities on the surface. Severe separation is indicated behind this turret, where the pressure recovery is little greater than that behind the circular cylinder.

Lower gun turret on Douglas XSB-2D-1 airplane.- As a further example that involves the method of distribution of doublets along the axis of a body of revolution moving normal to its axis, the pressure distribution over the lower gun turret of the Douglas XSB-2D-1 airplane is estimated. The form and location of this gun turret are shown in figure 21. The pressure distribution over the central profile (line 1, figs. 21 and 22) is obtained and the distributions over other lines from front to back are assumed to be quite similar. For a shape that does not differ too greatly from a body of revolution, this assumption is reasonable and has in other cases been found to agree well with experiment. (See reference 1, for instance.)

[redacted]

The turret was divided for computational purposes into front and rear parts. The pressures were assumed to be the same as if the turret were a half-body on a plane containing the surface of the fuselage immediately forward of and to the rear of the turret, with a stream velocity parallel to the plane. As shown in figure 23, the forward part of the turret profile can be approximated by an arc of the parabola

$$\frac{y}{c} = 0.744 \frac{x}{c}\left(1 - \frac{x}{c}\right)$$

With substitution of the slope

$$\frac{d(y/c)}{d(x/c)} = 0.744 - 1.488\frac{x}{c}$$

in equation (11), the velocity distribution

$$\frac{\Delta V}{V_o} \approx \frac{1}{\pi}\left[1.488 - \left(0.744 - 1.488\,\frac{x_o}{c}\right)\log_e\left(\frac{\frac{x_o}{c} - 1}{\frac{x_o}{c}}\right)\right]$$

shown in figure 23 is easily obtained.

The rear of the turret was approximated by a quarter-body of revolution with polar axis normal to the stream in the horizontal direction and with symmetry to the right and to the left. Velocity distribution was computed by the method of distributing doublets along the polar axis normal to the flow. (See reference 12.) The cross section normal to the stream, the central profile that is the approximation to the rear part of line 1 along the stream direction, and the required dimensions are shown in figure 24. The doublets of constant strength are indicated by the short, heavy lines along the axis; and, from equation (3) of reference 12, the potential for one doublet is

$$\Phi = \frac{\mu}{4\pi r}(\cos\theta'' - \cos\theta')\cos\phi$$

[redacted]

By symmetry, the velocity on the surface at $l = 0$ must lie along the central profile (fig. 24(b)) in the plane of the stream velocity. Because the largest and smallest velocities on the body occur along this profile, this distribution is of greatest interest. The velocity due to one doublet, the i doublet, is

$$\Delta V_i = \frac{1}{r_o}\frac{\partial \Phi}{\partial \phi} = \frac{-\mu_i}{4\pi r_o^2}(\cos \theta_i'' - \cos \theta_i') \sin \phi$$

Reference 12 shows that as an approximation the doublet intensity μ_i can be written

$$\mu_i = 2\pi r_i^2 V_o$$

The velocity increments ΔV_i are parallel and, with the substitution for μ_i, can be added to give

$$\frac{\Delta V}{V_o} \approx \frac{1}{2}\sum\left(\frac{r_i}{r_o}\right)^2 (\cos \theta_i' - \cos \theta_i'') \sin \phi$$

The component of the stream velocity V_o in the direction of the profile is $V_o \sin \phi$ and the total velocity is therefore

$$\frac{V}{V_o} = \left[1 + \frac{1}{2}\sum\left(\frac{r_i}{r_o}\right)^2 (\cos \theta_i' - \cos \theta_i'')\right] \sin \phi$$

From the dimensions given in figure 24, the computation of $\Delta V/V_o$ is indicated as follows:

i	$\left(\frac{r_i}{r_o}\right)^2$	cos θ_i'	cos θ_i''	$\left(\frac{r_i}{r_o}\right)^2$ (cos θ_i' - cos θ_i'')
-3	0.347	0.717	0.592	0.0434
-2	.779	.592	.403	.1472
-1	1.000	.403	.145	.258
0	1.000	.145	-.145	.290
1	1.000	-.145	-.403	.258
2	.779	-.403	-.592	.147
3	.347	-.592	-.717	.0434
	$\sum\left(\frac{r_i}{r_o}\right)^2(\cos\theta_i' - \cos\theta_i'') = 1.187$			

The velocity is therefore

$$\frac{V}{V_o} = \left(1 + \frac{1.187}{2}\right)\sin\phi = 1.594\sin\phi$$

which seems reasonable in comparison with the value $1.5\sin\phi$ for the sphere. The position along the stream direction x at which the velocity occurs is obtained with $\frac{x}{r_o} = \sin\phi$.

From the velocity distributions thus calculated for the front and rear portions of the turret, the corresponding pressure distributions were obtained by equation (2) and were then joined at the center to give the solid line in figure 22. Some adjustment of pressures was necessary to effect this junction.

For the turret in the guns-abeam position, the pressure distribution over the cylindrical surface (line 2, fig. 21) was estimated by assuming a circular cylinder projecting from a wall. The dimensions are such that $\cos\theta = 0.452$. Substitution of this value in equation (23) gives the velocity on the surface of the cylindrical gun turret near the fuselage. The pressures are thereby determined and are shown as the dashed line in figure 22.

[redacted]

The remarks concerning the effects of interference, boundary layer, and separation on the SB2A-1 turret also apply to the XSB-2D-1 turret. For the reasons discussed in reference to the SB2A-1 airplane, no compressibility correction has been applied. The turret does not project from the fuselage so far as was assumed in the calculations. For this reason, the estimated pressures should be more conservative than would otherwise have been the case. No experimental data are available for comparison.

Analysis and Discussion

The agreement between estimated and measured pressures generally is better than had been expected and it appears that, if allowance is made for the effects of interference and separation, calculations based on the potential-flow theory give a satisfactory indication of the maximum loads. The agreement is good for the Martin and Maxson turrets, which approach forms for which the potential flow can be accurately calculated. In other cases, the actual pressures may depart widely from the theoretical values. The reasons for this divergence from the calculated values - which are connected with departure of the shapes from those assumed, with compressibility effects, with interference, and with separation and other boundary-layer effects - are now discussed. The experimental data available are analyzed and compared with theoretical values to determine, at least qualitatively, the modifications that should be made to calculated pressure distributions in order to approximate more closely the actual values. The application of pressure distributions to the estimation of loads is briefly considered. The following additional figures are introduced:

Pressure data obtained in the NACA 8-foot high-speed tunnel (unpublished) on approximately hemispherical turrets at different locations on a fuselage are shown in figure 25. The orifices at which these pressure data were obtained were located at the tops of turrets C, D, and E and at the side of turret C, where velocities approaching the maximum should occur. The variation of pressure coefficient P with stream Mach number M is compared with the theoretical variation given by the factor $\frac{1}{\sqrt{1 - M^2}}$. In figures 25 to 27, the curve of critical pressure coefficient P_{cr} - that is, the

[redacted]

pressure coefficient corresponding outside the boundary layer to the attainment of the local speed of sound is shown to indicate the critical speeds of the turrets. The critical Mach number M_{cr} is the Mach number at which the pressure-coefficient curve intersects the P_{cr}-curve.

Figure 26 shows a comparison between the pressures at the top of two spherical-segment turrets A and D, both in the forward location of turret A as shown in figure 11(b) and projecting different portions of the radius above the fuselage. These pressures are compared with the theoretical pressures for the sphere including the variation with Mach number given by the factor $\frac{1}{\sqrt{1 - M^2}}$.

A comparison is given in figure 27 between pressure coefficients at various positions on the faired turret E of reference 16 and those on a thicker faired turret F, both in the location of turret B shown in figure 11(c). The variation with Mach number is shown and compared with the theoretical variation.

Figure 28, for which the data are taken from reference 1, shows the pressure change with Mach number at four different points on windshields representing bodies of three different types: the 3-1-1, which has a blunt tail; the 7-3-4, which is characterized by a sharp corner at the nose and by a long, faired tail; and the X-1, which is well streamlined.

Departure from forms for which potential flow can be calculated.- The shape of a protuberance is usually such that the potential flow cannot be exactly computed. Experiment is therefore needed to determine the effect of systematic departure from forms for which the potential flow is calculable, such as variation in segment of a sphere from the half-body or variation in thickness of a body. The effect of these variations is indicated in figures 26 and 27. The pressures vary qualitatively as might have been expected; that is, larger peaks are obtained for thicker bodies. The data are insufficient, however, to define any quantitative relations.

[redacted]

Figures 25 and 26 indicate that, unless considerable interference is present, the limiting pressure on a spherical segment less than a hemisphere may be taken as that on the sphere.

Compressibility.- The effect of compressibility on the pressure coefficients over protuberances cannot be accurately estimated although a qualitative estimate of the nature of the change of pressure with Mach number may be obtained. The theoretical variation shown in equations (3) and (4) and derived in references 2 and 3, respectively, strictly applies only to potential flow. The actual variation may be greater or less than the theoretical variation and may even be opposite in sign. For protuberances, which are usually influenced by boundary-layer development forward of the protuberance and by separation of the flow, the theory is less useful than for airfoils, for which the flow generally approaches more nearly the potential. As shown in figures 14, 16, and 25 to 28, the peak negative pressures generally increase with Mach number more rapidly on well-faired bodies located on the forward part of the wing or fuselage than on blunt bodies located near the tail. A detailed examination of the experimental data available indicates how and why the pressure coefficients in different positions on protuberances change with Mach number.

On the low-cambered turret A of figure 14, the peak pressures change with Mach number approximately as predicted by the Glauert-Prandtl theory. At the rear of such a body, the pressures decrease because of an increase in severity of separation - a compressibility effect that has been observed in other tests (unpublished). The compressibility effects on the faired turret B of figure 16 are similar to those on turret A, except that for turret B the positive pressure coefficient at the rear, which should theoretically have increased, was maintained constant by the slight separation of the flow or thickening of the boundary layer. The effective change in shape of the form was apparently sufficient to cause a slight decrease in the negative pressure coefficient at the 5-inch station.

Figure 25 shows different compressibility effects on the pressures at the top and side of approximately hemispherical turrets that depend on interference and the boundary-layer development ahead of the turret.

Turret C is subject to considerable interference from the windshield just downstream. This interference decreases the velocities and prevents the increase in negative pressure coefficient with Mach number that would otherwise occur. Turret D, on the other hand, is placed in a region in which the interference may be expected to increase the velocities; and the increase with Mach number of the top negative pressure coefficient approximates the theoretical increase up to the critical speed, after which it increases sharply for a short Mach number range. Turret E, which is located far back on the fuselage and therefore subject to considerable interference from the boundary layer, shows small change in the pressure coefficient with Mach number.

The turrets of figure 26 were located in a region in which the boundary layer on the fuselage must have been very thin. In addition, considerable interference was possible; the possible effect of interference in increasing the change of pressure coefficient with Mach number is discussed in reference 1. The peak negative pressure coefficient on the approximately hemispherical turret D increased with Mach number about according to theory up to the critical speed and more rapidly thereafter. The increase on the lower-cambered turret A approximates the theoretical increase.

The compressibility effect on the pressures of turret B has already been noted in figure 27. The variation of the peak negative pressure coefficients appears to agree closely with the theoretical variation. For the thicker turret F, the separation should be more severe; this fact is probably the reason that the pressure coefficient at the top increases less rapidly with Mach number than the theory indicates. Farther back on the turret, the change in effective shape due to separation produces a large decrease in negative pressure coefficient as the Mach number is increased.

The effect of compressibility on pressure coefficients at points on bodies of three different types (from reference 1) is shown in figure 28. For the well-streamlined X-1 body, the pressures at points b and d agree with the theoretical change with Mach number; at point a, the peak increases more rapidly than the theoretical values; and, at point c, the effect of thickening boundary layer in decreasing the pressure is seen. On the 7-3-4 body, which has a

[redacted]

well-faired tail and a sharp corner between the windshield and the hood, the pressure at point d agrees with the theoretical variation, the pressure at point c shows the effect of thickening boundary layer, and the negative pressure coefficients at points a and b a short distance behind the point of separation decrease before they start to rise with Mach number. On the 3-1-1 body, which has a blunt tail, the pressures at points b and d change about as theoretically predicted, the pressure at point a somewhat ahead of the separation point fails for the most part to decrease as fast as indicated by the theory, and the pressure at point c on the tail decreases greatly behind the point at which separation probably occurs.

The effect on pressure coefficients of change in Mach number is seen to be different for different points and for different bodies. For roughly similar shapes in similar locations, the corresponding variations with Mach number may be assumed.

The effect of compressibility on the pressures over a protuberance obviously depends on the Reynolds number of the protuberance and of the body on which it is placed, inasmuch as the type of flow must be a function of the Reynolds number. Compressibility effects also depend on the relative size of the protuberance in relation to the body on which it is placed, because interference and boundary-layer effects are different for different relative dimensions.

From the experimental data, the following principles that are useful in a qualitative estimation of the change of pressure coefficient with Mach number may be derived:

(1) Over the greater part of well-faired bodies that are not too thick and are relatively free from boundary-layer and velocity interference from other bodies, the theoretical change of pressure coefficient with Mach number may be assumed. The factor $\frac{1}{\sqrt{1 - M^2}}$ expresses the change with sufficient accuracy. The negative pressure peaks may be assumed to increase somewhat more rapidly than this factor indicates.

[redacted]

(2) Separation of the flow, which regularly occurs from the rear of blunt forms - such as the sphere and the circular cylinder - and to a less degree from less blunt bodies, is likely to become more severe with increase in Mach number. The resulting change in the effective shape of the body may produce an increase (as compared with the theoretical decrease) of the pressure coefficients near the beginning of the separated region and a decrease (more-negative pressure coefficients) near the tail. Even on moderately thin faired bodies, something of this effect may appear; whereas, on bodies with short tails, a large decrease in the negative pressure coefficients just forward of the tail and a considerable increase in the negative pressure coefficients at the rear may occur.

(3) Interference that increases the velocities is likely to cause a further increase in negative pressure coefficients with Mach number, whereas interference that decreases the velocities is likely to have the opposite effect.

(4) If any considerable part of the protuberance lies within the boundary layer produced on the body forward of the protuberance, the change in pressure coefficient with Mach number is likely to be different from the change that would occur if no boundary layer existed. The pressure peaks may be smaller and separation effects may be introduced.

(5) If a critical Reynolds number occurs within the Mach number range or if a considerable change in pressure coefficient with Reynolds number is otherwise to be expected, the resulting effect on the change in pressure coefficient with Mach number must be accounted for.

The foregoing discussion holds for Mach numbers less than the critical. Above the critical Mach number, still less is known about the pressures to be expected. Outside the region of supersonic speeds, the pressure change is much the same as at subcritical Mach numbers. The supersonic region commonly spreads rearward as the Mach number is increased, and the negative pressure peak usually increases and broadens toward the rear. As the shock wave develops with its large unfavorable pressure gradient, separation is likely to occur and produce the pressure changes already discussed.

[redacted]

The negative pressure coefficients cannot in any case continue indefinitely to increase with Mach number, and a tendency to decrease at the highest Mach numbers is already apparent in some of the curves in figures 25 and 26. An absolute limit imposed by the condition that the local static pressure be zero is given by $(-P)_{max} = \frac{2}{\gamma M^2}$. The experimental data available indicate a limit less than given by this relation. Up to a Mach number of 0.7?, however, the changes in pressure coefficients likely to be encountered on protuberances may be estimated by the methods herein presented.

In order to estimate with quantitative accuracy the effect of compressibility on the pressure distributions over protuberances, extensive systematic experimentation is necessary.

Interference.- For cases in which the interference cannot be expressed by simply adding in the induced velocities due to the interfering bodies, an estimation at least qualitatively correct may still be obtained. It is reasonably certain, for instance, that a canopy in front of a gun turret can have only the effect of reducing the velocities and thereby the pressure peaks.

Figure 25 illustrates the difference in interference effects for turrets in different locations on the fuselage and for different angles of attack of the wing and fuselage. Turret C is subject to a reduction in velocity due to the hump in the fuselage immediately behind it and, in addition, the accompanying unfavorable pressure gradient may be expected to precipitate earlier separation than would otherwise occur. As seen in figure 25, the negative pressure coefficients on the top of turret C were much smaller than on turret D, which was located in a region of increased velocity due to both wing and fuselage. Turret E is so located that the velocity interference should be small but, with most of the fuselage forward of the turret, the boundary-layer interference must have been considerable. The negative pressure coefficients are only moderately large. The change in pressure coefficient with angle of attack is appreciable. A rough estimate of the interference could be obtained by adding the induced velocities due to the wing and fuselage as in reference 1.

[redacted]

The velocity interference on the central part of a fuselage commonly amounts to about $\frac{\Delta V}{V_o} = 0.10$. A rough estimate of the induced velocity can be obtained by fitting an equivalent prolate spheroid to the fuselage as described in the section entitled "Methods" and in reference 1.

The wing is approximately a two-dimensional form and thus may cause relatively large interfering velocities. If a protuberance is located near the velocity peak on a wing, therefore, the pressures may be widely different from those on the same protuberance not subject to the interference; in addition, the change in pressure with change in Mach number or wing angle of attack may be large.

It may be necessary in some cases to determine the interference effect of a protuberance on the loads over surrounding surfaces. The induced velocities generally decrease very rapidly with increase in distance from the surface. The decrease of the peak velocity increment is shown for a wing and for prolate spheroids in figures 36 and 37, respectively, of reference 1. The methods given in the appendix of reference 1 can be used to estimate the interference due to a protuberance. If an equivalent prolate spheroid can be fitted to the protuberance, the maximum interference velocities can be estimated from figure 37 of reference 1. If more detailed information is needed, however, a velocity-contour chart such as that of figure 35 of reference 1 can be prepared for a body approximating the protuberance in shape. For simple shapes, such as the sphere or oblate spheroid, velocity contours are easily obtained from the potential theory. Additional experiment is needed to permit very accurate estimates of the effects of interference.

Surface irregularities.- The theoretical pressure distributions are calculated for smooth bodies, but in practice the surface is usually broken by ribs, joints, waves, or other irregularities; as a result, peaks and valleys appear in the pressure-distribution curve. Such an irregular pressure distribution is given by the experimental data shown in figure 19. The most obvious surface irregularities in this case were the ribs of the turret. Estimated pressure distributions should be made sufficiently conservative to allow for the effects of these irregularities.

[redacted]

Separation and pressure behind a protuberance.- Most protuberances are sufficiently blunt at the tail that the flow fails to some extent to follow the surface. This separation of the flow is aggravated by the boundary layer developed on the surface forward of the protuberance with the result that separation becomes more severe as the protuberance is placed farther back from the nose of the fuselage or other body on which it is situated.

Although separation does not usually increase the severity of the loads, it greatly increases the drag of the protuberance and should therefore be prevented by a fairing if conveniently possible. In the case of gun turrets, a method that might be used while the advantages of symmetrical turrets are retained is to install retractable fairings behind the turrets. The effect of fairing on separation is shown in a comparison of the experimental data given in figures 12, 14, 16, and 19. The use of faired turrets appears to give little advantage over symmetrical turrets unless the fairing is sufficient to prevent any considerable separation. If the flow becomes unsymmetrical when the turret is rotated from the stowed position, local loads may be substantially increased. If sharp corners are thus exposed, the pressures may be impossible to estimate and the peak negative pressures may become very high.

At sharp outside corners, the flow separates either completely or with a bubble about which the flow later closes in. A method of estimating the pressures near sharp corners has been suggested in the section entitled "Estimation by Comparison." It is pointed out in reference 1 on pages 12 and 13 that outside corners with radii of curvatures less than approximately 25 percent of the height of the protuberance may be considered sharp.

Separation changes the effective shape of a body in such a way that the pressure peaks influenced by the separation are reduced and the pressure on the rear of the original form is decreased. At the rear of the faired turret of figure 16, therefore, the pressure coefficient is positive; whereas, on the rear of the more severe turret of figure 14, for which a greater pressure recovery is indicated, separation has reduced the pressure coefficient to zero. Behind the still

[redacted]

more severe forms of figures 12 and 19, the pressure coefficients at the rear are negative. From these experimental data and from the known values of the pressure coefficient on the rear of spheres and circular cylinders, a rough estimate of the pressures behind protuberances can be made; but it is evident that, in order to judge accurately whether separation will occur and what pressures will then exist, much systematic experimentation is required.

The effect of compressibility in precipitating or increasing the severity of separation has already been noted.

Estimation of loads.- From the pressure distributions, estimated or measured, the loads can be determined provided the internal pressures are known. The internal-pressure coefficient may be positive if the protuberance is vented to a high-pressure region, as about the nose or tail of the fuselage, but is more likely to be negative because leaks regularly occur to the low-pressure region in which a protuberance is usually placed, such as leaks around the sliding canopy, through other cracks, or through holes in the surface. Because the external pressures vary with angle of attack or the positions of the leaks change with angle of gun turret, the internal pressures also vary. Since negative pressure coefficients up to $P = -0.40$ often occur on a fuselage, similar pressures may be expected inside canopies or gun turrets. In low-speed tests of the Grumman XTBF-1 airplane (unpublished), for example, internal-pressure coefficients of -0.13 were found in the canopy while, in the symmetrical Martin turret tested, the pressure coefficient varied from -0.02 to -0.11 depending on the angular position of the turret and angle of attack of the airplane; similarly, in the unsymmetrical Grumman turret with which the airplane was originally equipped, the internal-pressure coefficient varied between 0 and -0.06. For the Brewster XSB2A-1 airplane in flight (unpublished), internal pressures in the gun turret varied from $P = -0.20$ to $P = -0.38$; inside the cockpit canopy of the SB2A-4 airplane, very low pressure coefficients of -0.30 to -0.40 were found. Because of differences in leakage, the internal pressures are likely to be different from time to time, even for the same airplane, unless the

[redacted]

enclosures are sealed. It is evident that, because of low internal pressures, jettison may be impossible even if a protuberance is designed to be released. An increase of internal pressure could be realized by venting to the tail of the fuselage.

CONCLUSIONS

1. By the methods given in the present report, pressure distributions can be estimated for use in calculating loads.

2. If allowance is made for the effects of interference and separation, calculations based on the potential-flow theory give a satisfactory indication of the maximum pressures to be expected.

3. For shapes about which the potential flow is not exactly calculable, the pressures may be estimated by various approximate methods presented or by comparison with experiment.

4. Compressibility and interference effects and the effects of departure from potential flow, including separation, can be estimated by a combination of theoretical methods presented and by comparison with experiment.

5. In order to estimate the loads, the pressure inside the body as well as the external-pressure distribution must be known.

6. Further experimental investigation is needed to determine the effects of interference, compressibility, separation, and systematic changes in form.

Langley Memorial Aeronautical Laboratory,
National Advisory Committee for Aeronautics,
Langley Field, Va.

[redacted]

REFERENCES

1. Delano, James B., and Wright, Ray H.: Investigation of Drag and Pressure Distribution of Windshields at High Speeds. NACA ARR, Jan. 1942.

2. Prandtl, L.: General Considerations on the Flow of Compressible Fluids. NACA TM No. 805, 1936.

3. von Kármán, Th.: Compressibility Effects in Aerodynamics. Jour. Aero. Sci., vol. 8, no. 9, July 1941, pp. 337-356.

4. von Doenhoff, Albert E.: A Method of Rapidly Estimating the Position of the Laminar Separation Point. NACA TN No. 671, 1938.

5. von Doenhoff, Albert E., and Tetervin, Neal: Determination of General Relations for the Behavior of Turbulent Boundary Layers. NACA ACR No. 3G13, 1943.

6. Theodorsen, T., and Garrick, I.E.: General Potential Theory of Arbitrary Wing Sections. NACA Rep. No. 452, 1933.

7. Jones, Robert T., and Cohen, Doris: A Graphical Method of Determining Pressure Distribution in Two-Dimensional Flow. NACA Rep. No. 722, 1941.

8. Zahm, A.F.: Flow and Drag Formulas for Simple Quadrics. NACA Rep. No. 253, 1927.

9. Glauert, H.: A Generalised Type of Joukowski Aerofoil. R. & M. No. 911, British A.R.C., 1924.

10. Goldstein, S.: A Theory of Aerofoils of Small Thickness. Part I. Velocity Distributions for Symmetrical Aerofoils. 5804, Ae. 1976 (revised), British A.R.C., May 14, 1942.

11. Lamb, Horace: Hydrodynamics. Sixth ed., Cambridge Univ. Press, 1932, pars. 107 and 109, pp. 142-146.

12. von Kármán, Th.: Calculation of Pressure Distribution on Airship Hulls. NACA TM No. 574, 1930.

[redacted]

13. Kaplan, Carl: On a New Method for Calculating the Potential Flow past a Body of Revolution. NACA ARR, July 1942.

14. Munk, Max M.: Fluid Mechanics, Pt. II. Vol. I of Aerodynamic Theory, div. C, W. F. Durand, ed., Julius Springer (Berlin), 1934.
Fluid Motion with Axial Symmetry, ch. V, sec. 6, p. 269.
Ellipsoid with Three Unequal Axes, ch. VIII, secs. 1-5, pp. 293-302.

15. Young, D. W., and Davis, E. L.: Drag and Pressure Distribution of Gun Turrets on a Model of the B-25 Fuselage. Five-Foot Wind Tunnel Test No. 30C. A.C.T.R. No. 4753, Materiel Command, Army Air Forces, April 10, 1942.

16. Mattson, Axel T.: Tests of a Large Spherical Turret and a Modified Turret on a Typical Bomber Fuselage. NACA ARR, Oct. 1942.

17. Fluid Motion Panel of the Aeronautical Research Committee and Others: Modern Developments in Fluid Dynamics. Vols. I and II. S. Goldstein, ed., Oxford at the Clarendon Press, 1938.

[redacted]

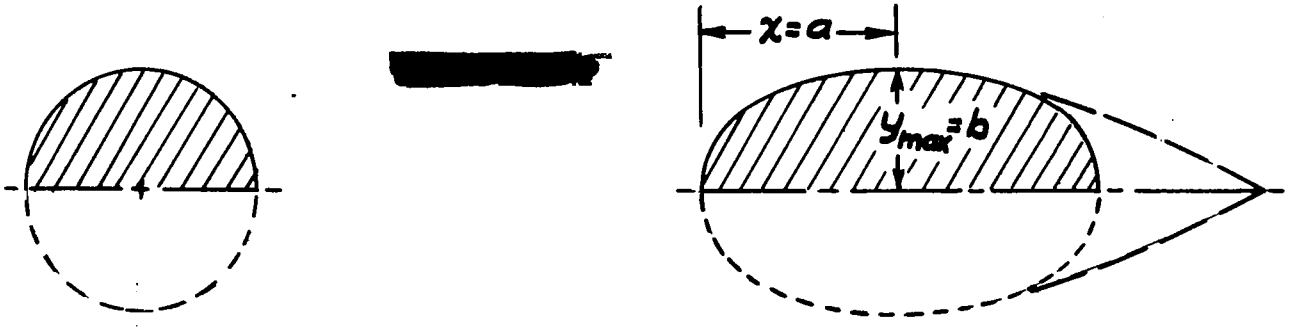

(a) Sphere or circular cylinder.

(c) Prolate spheroid or ellipse and body of revolution or airfoil with equivalent prolate spheroid or ellipse.

NATIONAL ADVISORY
COMMITTEE FOR AERONAUTICS.

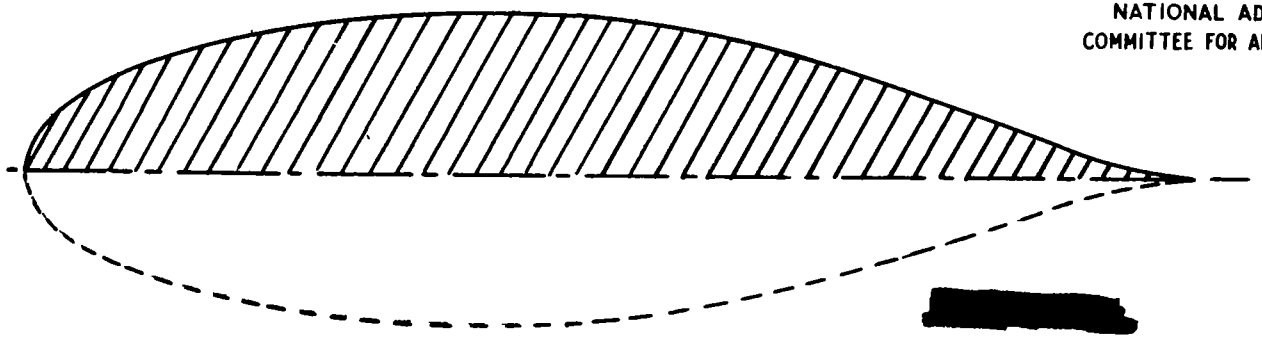

(b) Body of revolution or airfoil.

Figure 1.- Half-bodies resulting from section of symmetrical bodies at plane of symmetry.

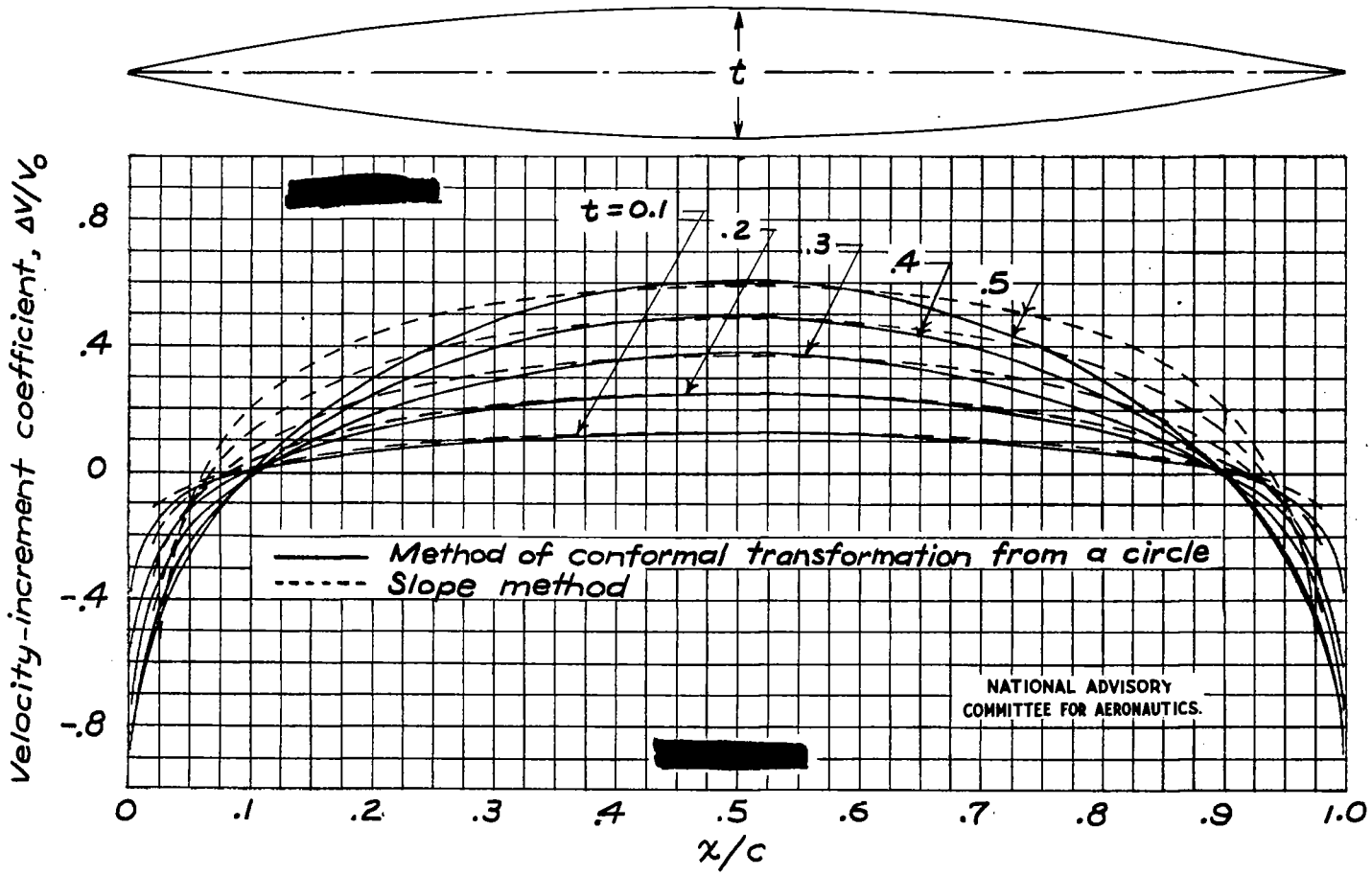

Figure 2.- Theoretical velocity distribution about double circular-arc symmetrical airfoils. t is thickness ratio.

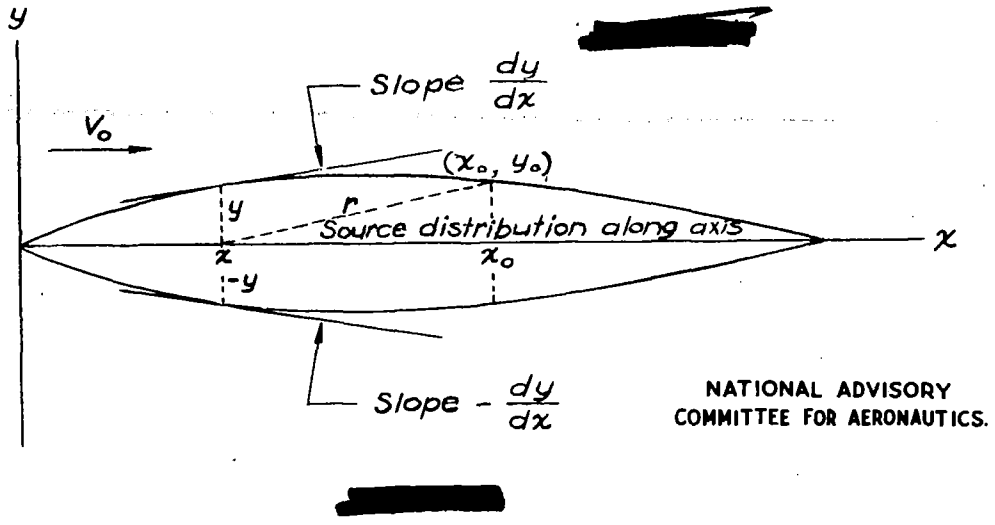

Figure 3.- Slope method for velocity calculation.

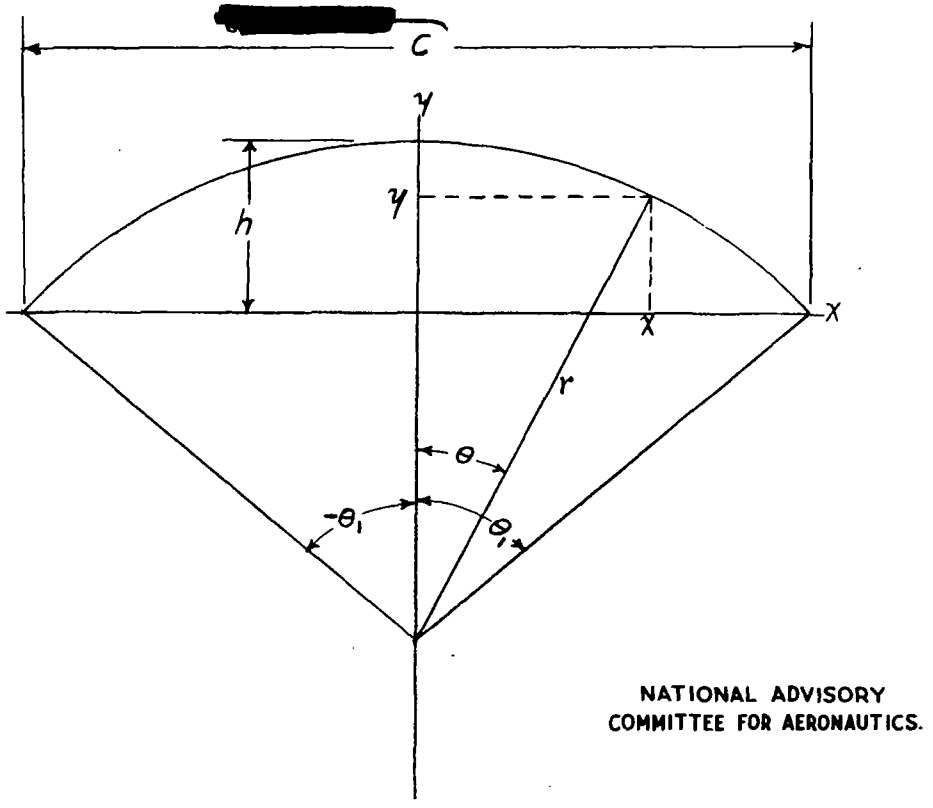

Figure 4.- Circular-arc profile.

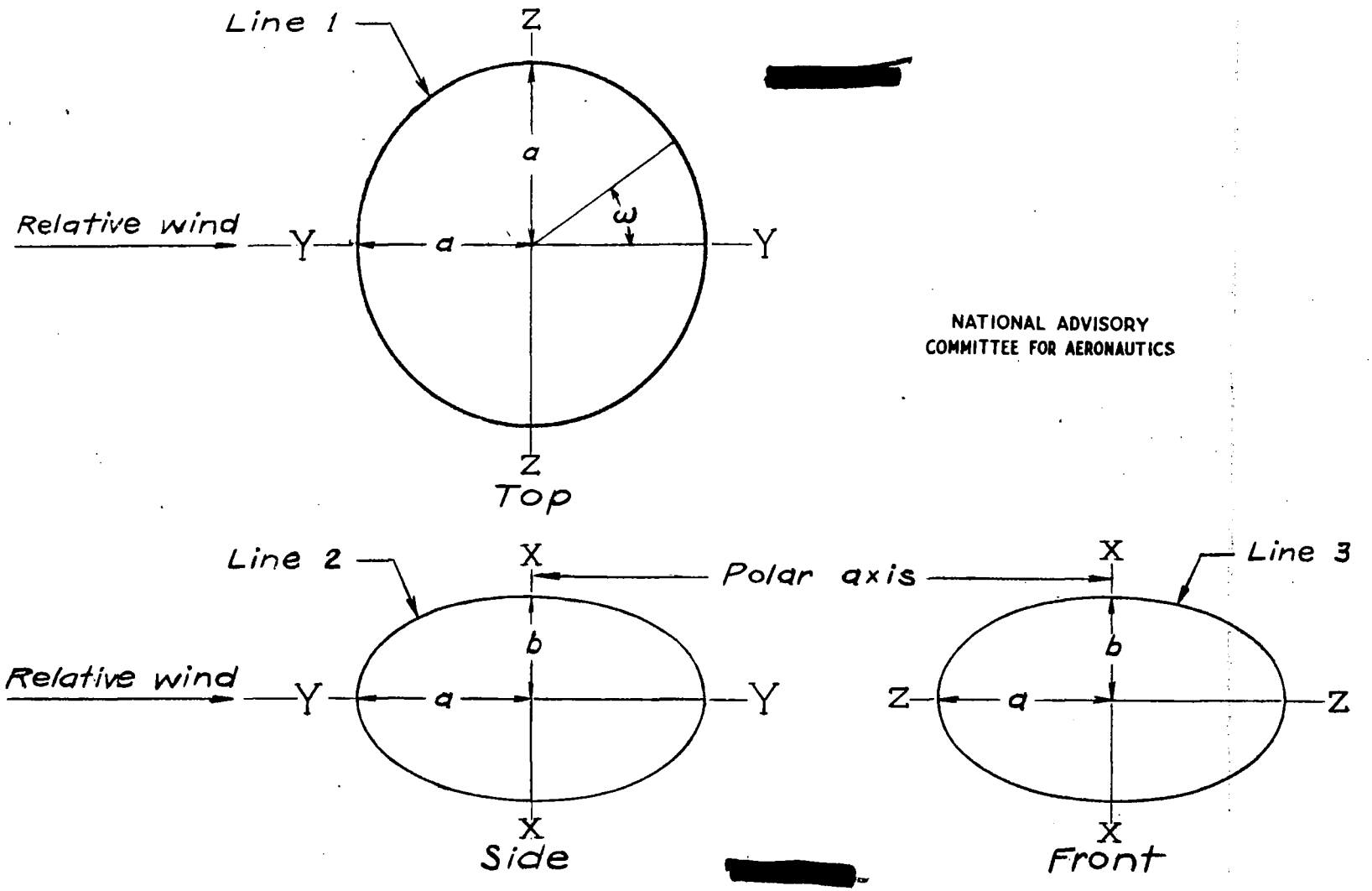

Figure 5.- Oblate spheroid moving normal to polar axis .

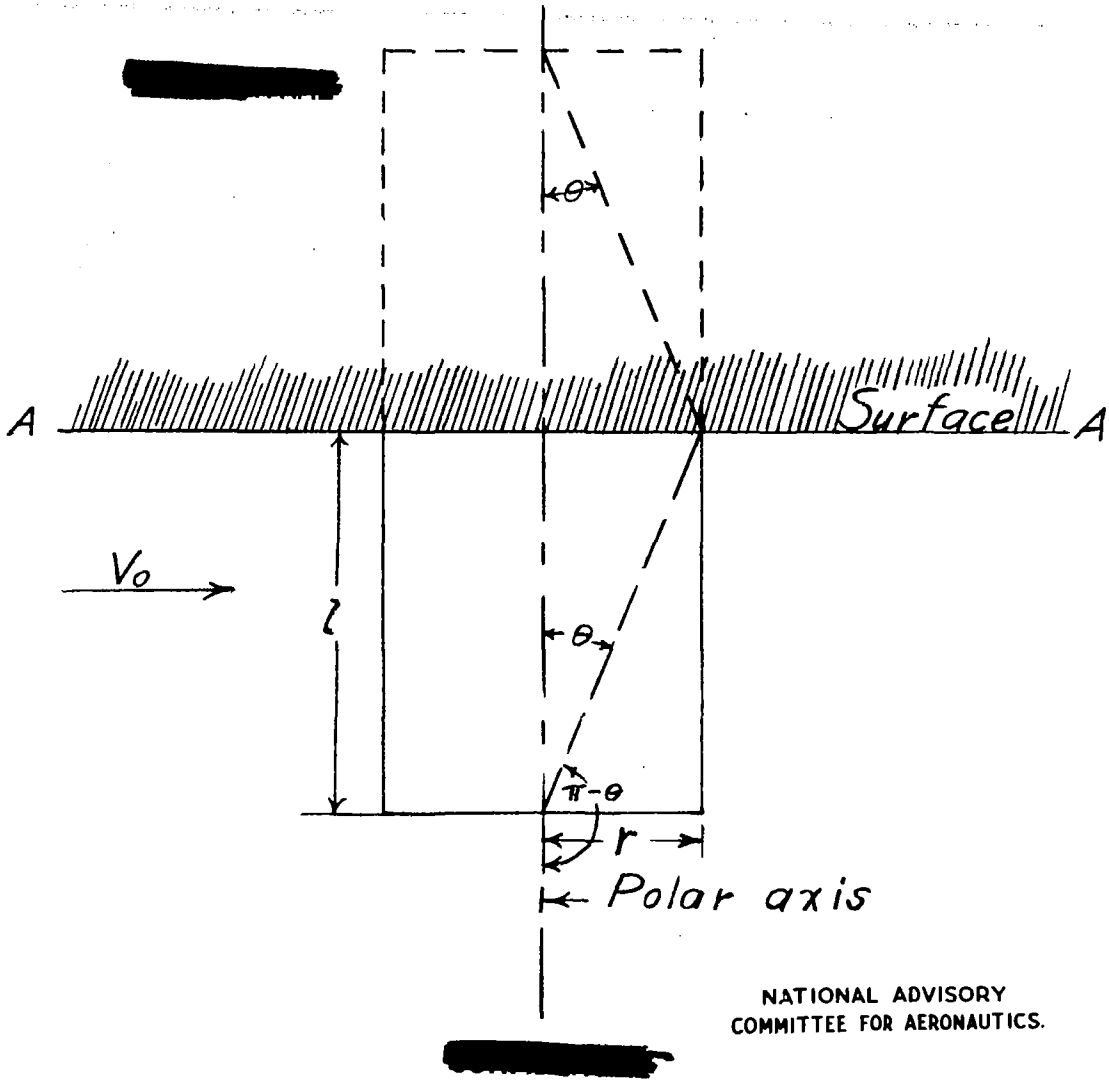

Figure 6.- Circular cylinder of finite length projecting from a surface.

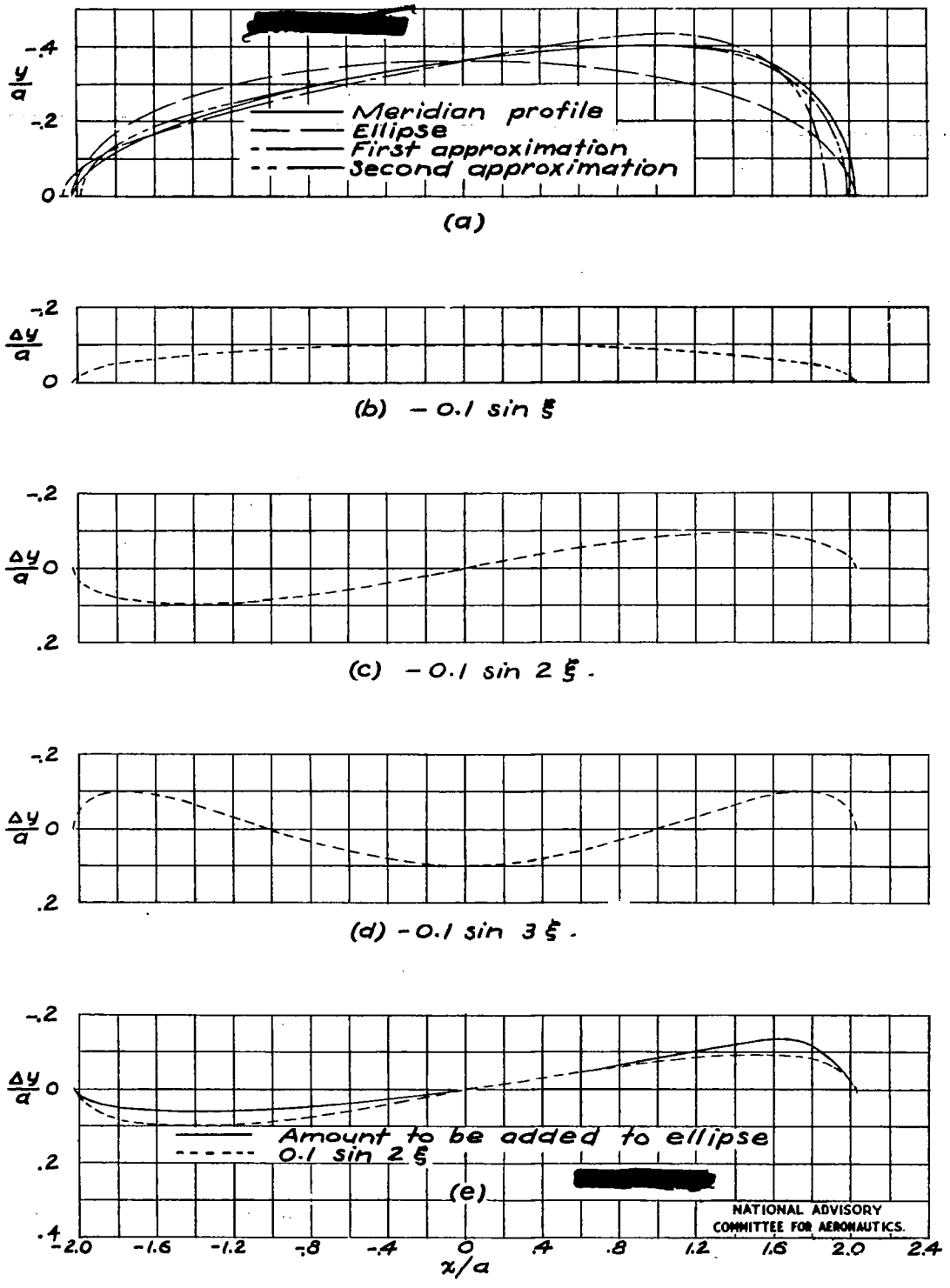

Figure 7. - Determination of the complex function for the conformal transformation of a circle into a profile approximating the meridian section of a body of revolution.

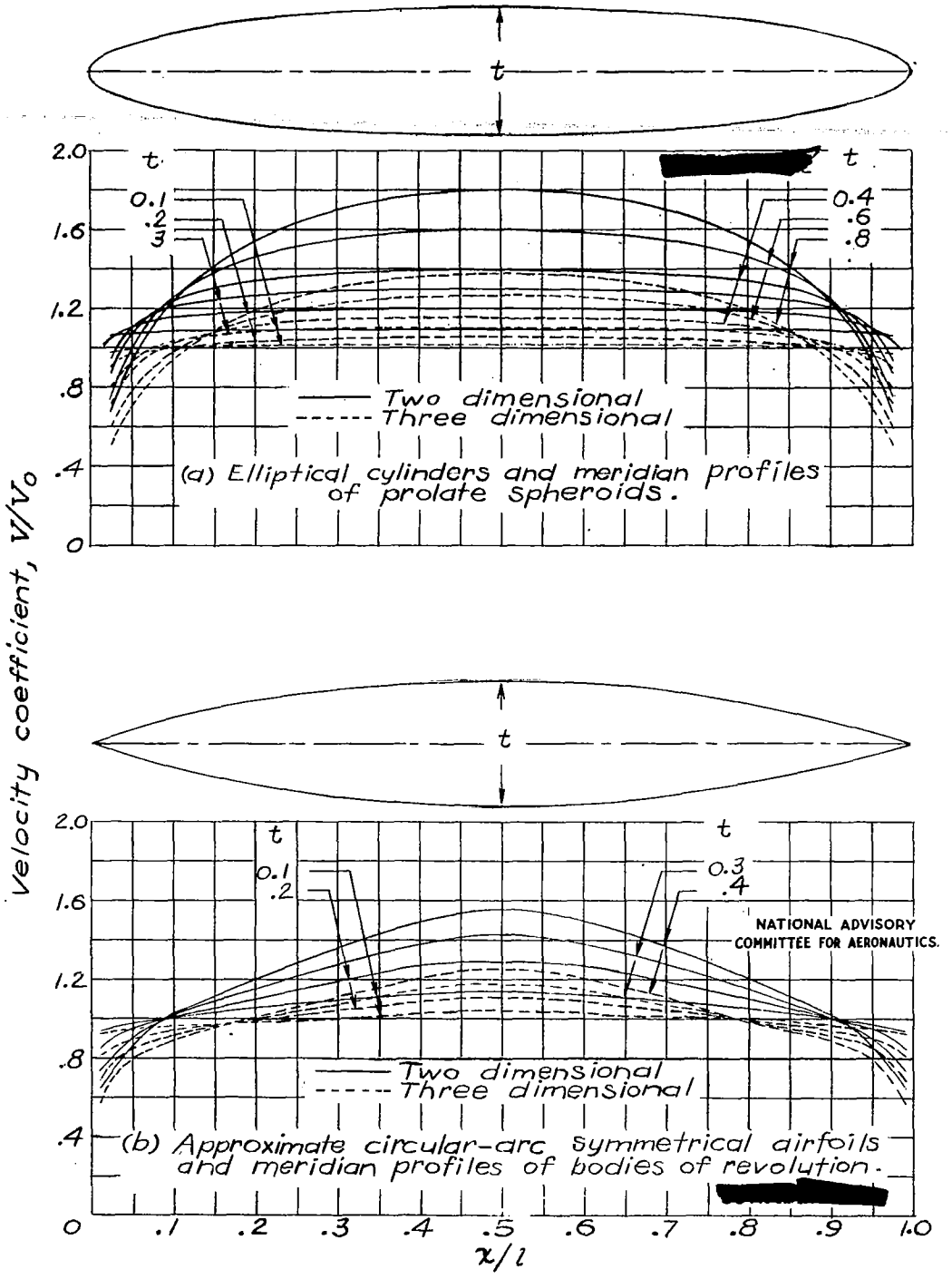

Figure 8.- Comparison of calculated velocity distributions over two-dimensional shapes with those over the corresponding bodies of revolution.

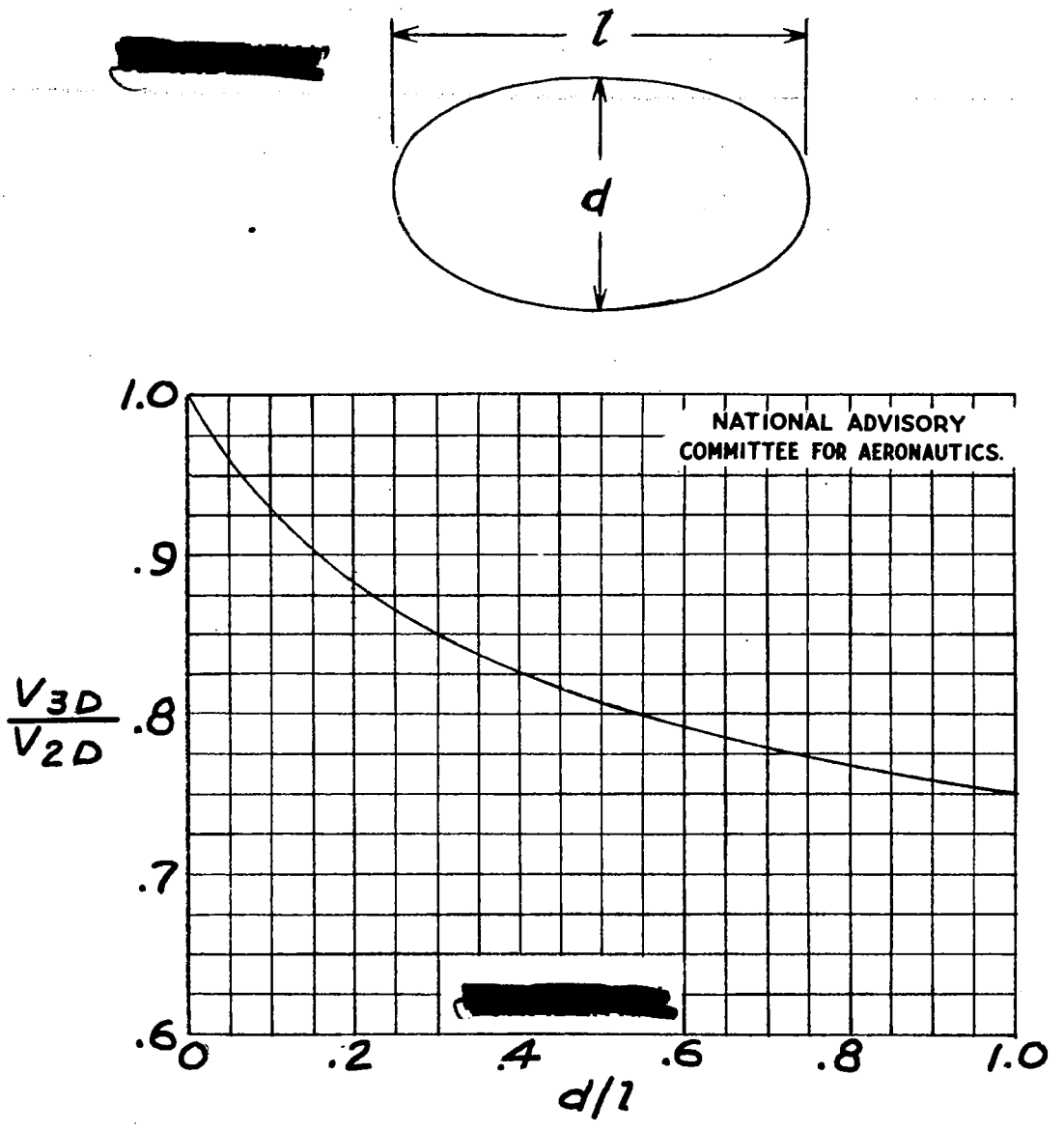

Figure 9.- Ratio of velocities on prolate spheroids to those on corresponding elliptic cylinders.

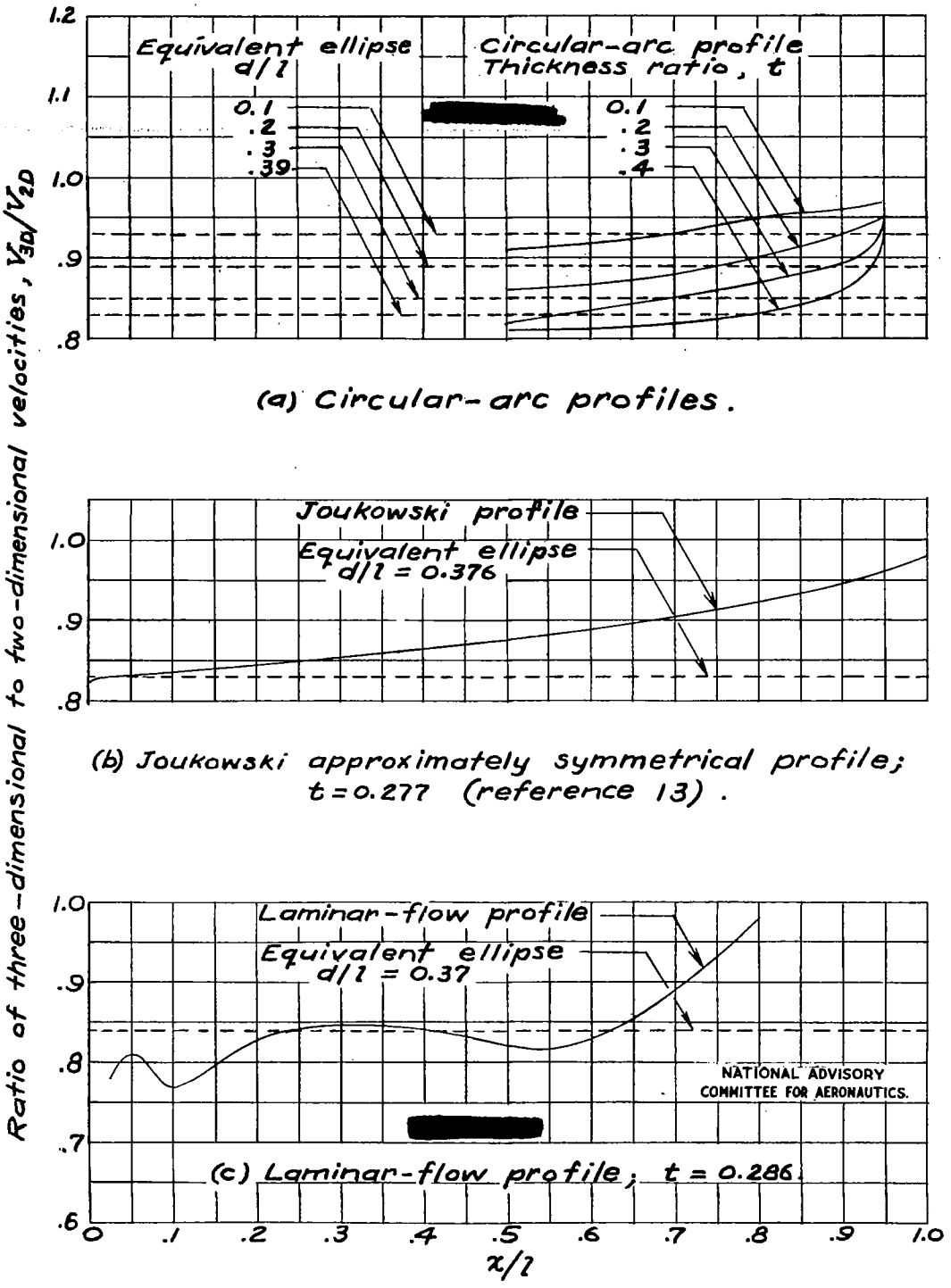

Figure 10.- Variation of the ratio of velocities in three-dimensional to those in two-dimensional flow over several bodies and their equivalent ellipses.

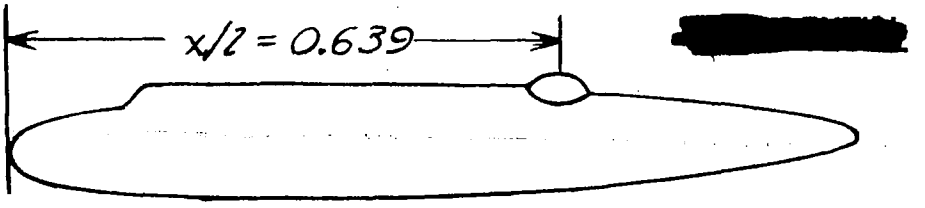

(a) Martin turret.

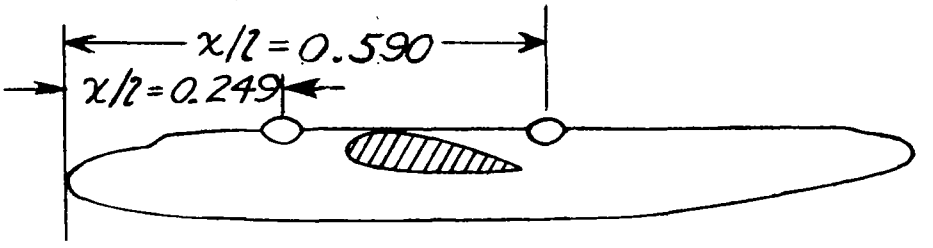

(b) Turret A in two locations.

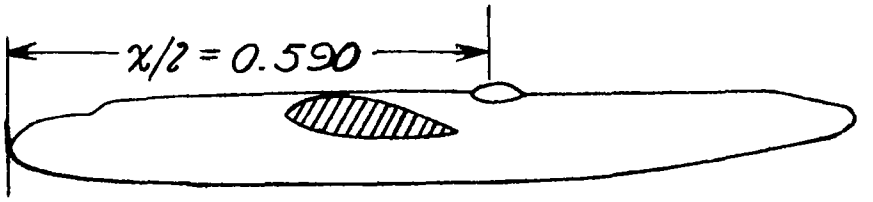

(c) Turret B.

NATIONAL ADVISORY
COMMITTEE FOR AERONAUTICS.

Figure 11.— Locations of the Martin turret and turrets A and B on fuselage.

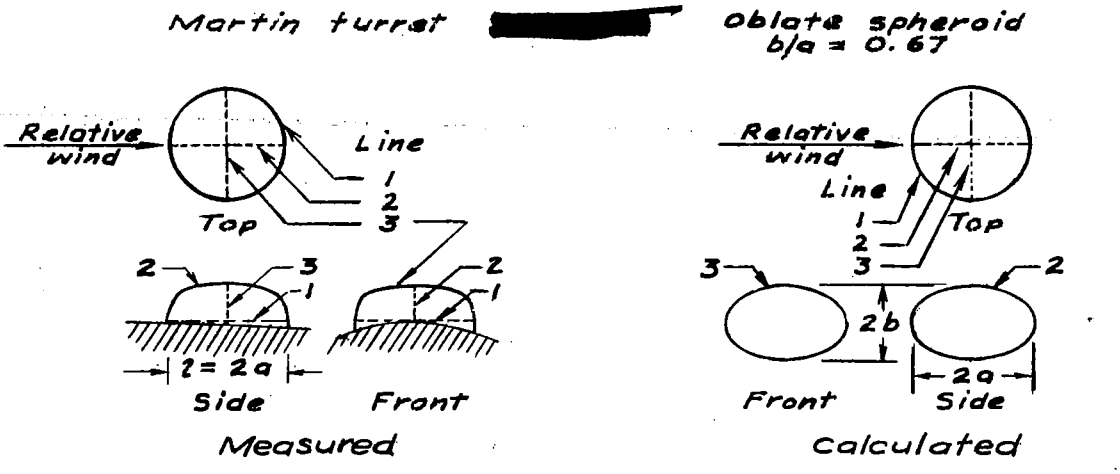

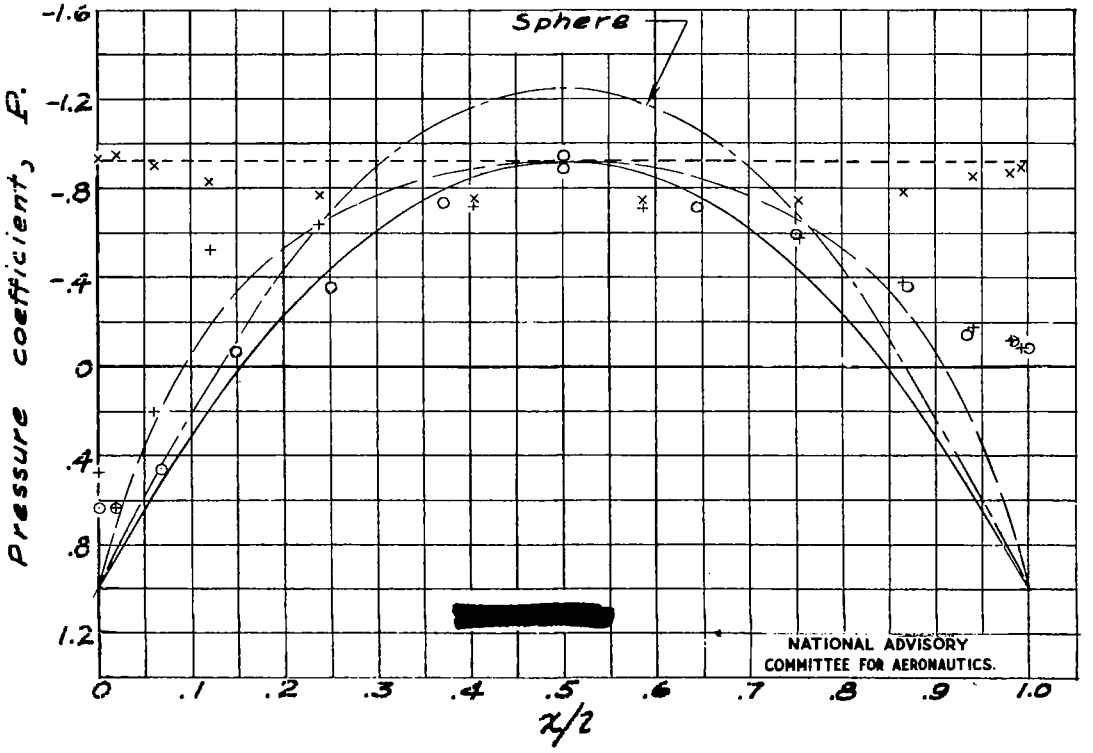

Figure 12.—Comparison of measured pressures on the Martin turret (reference 15) with calculated values on an equivalent oblate spheroid and on a sphere.

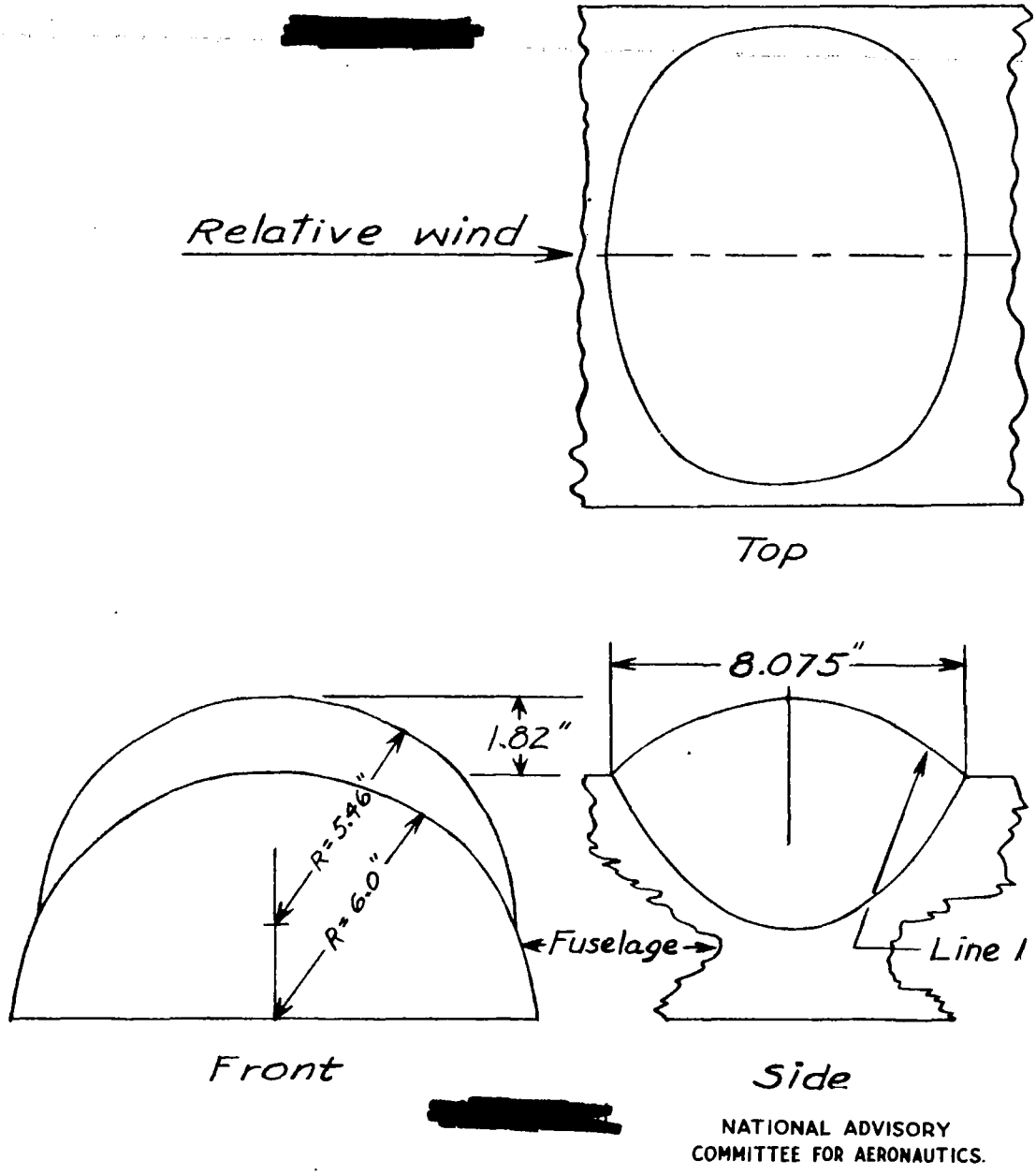

Figure 13.— Turret A details.

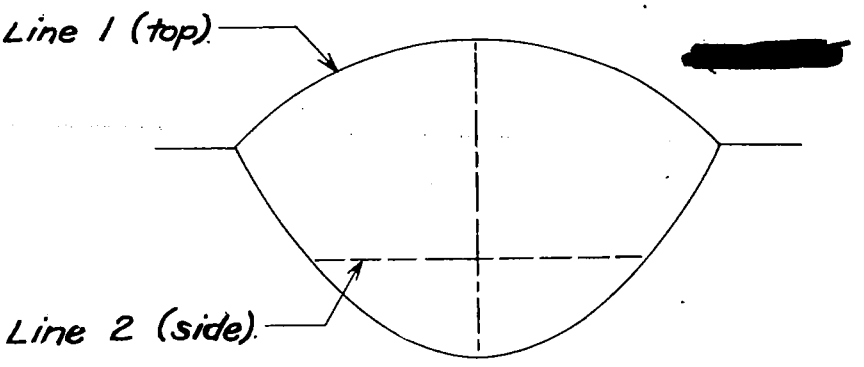

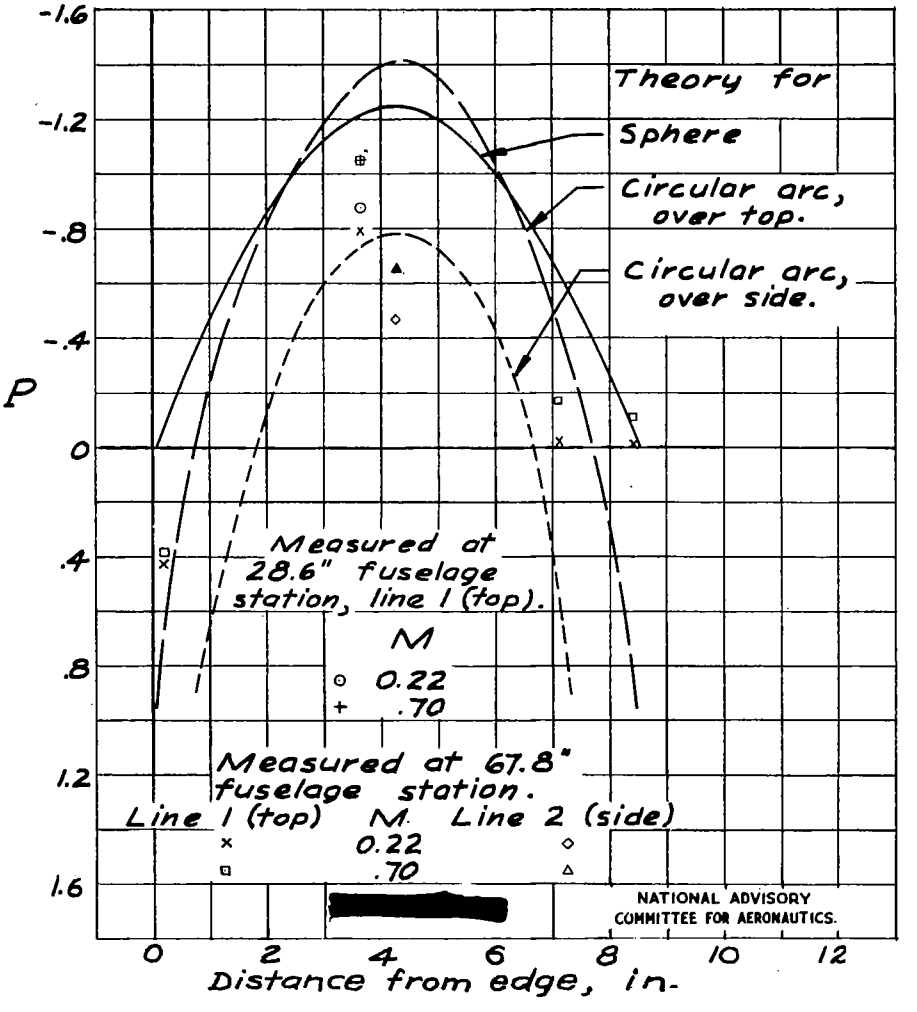

Figure 14.- Comparison of measured pressures on turret A of reference 16 with theoretical pressures on sphere and circular arcs. $\alpha = 3°$.

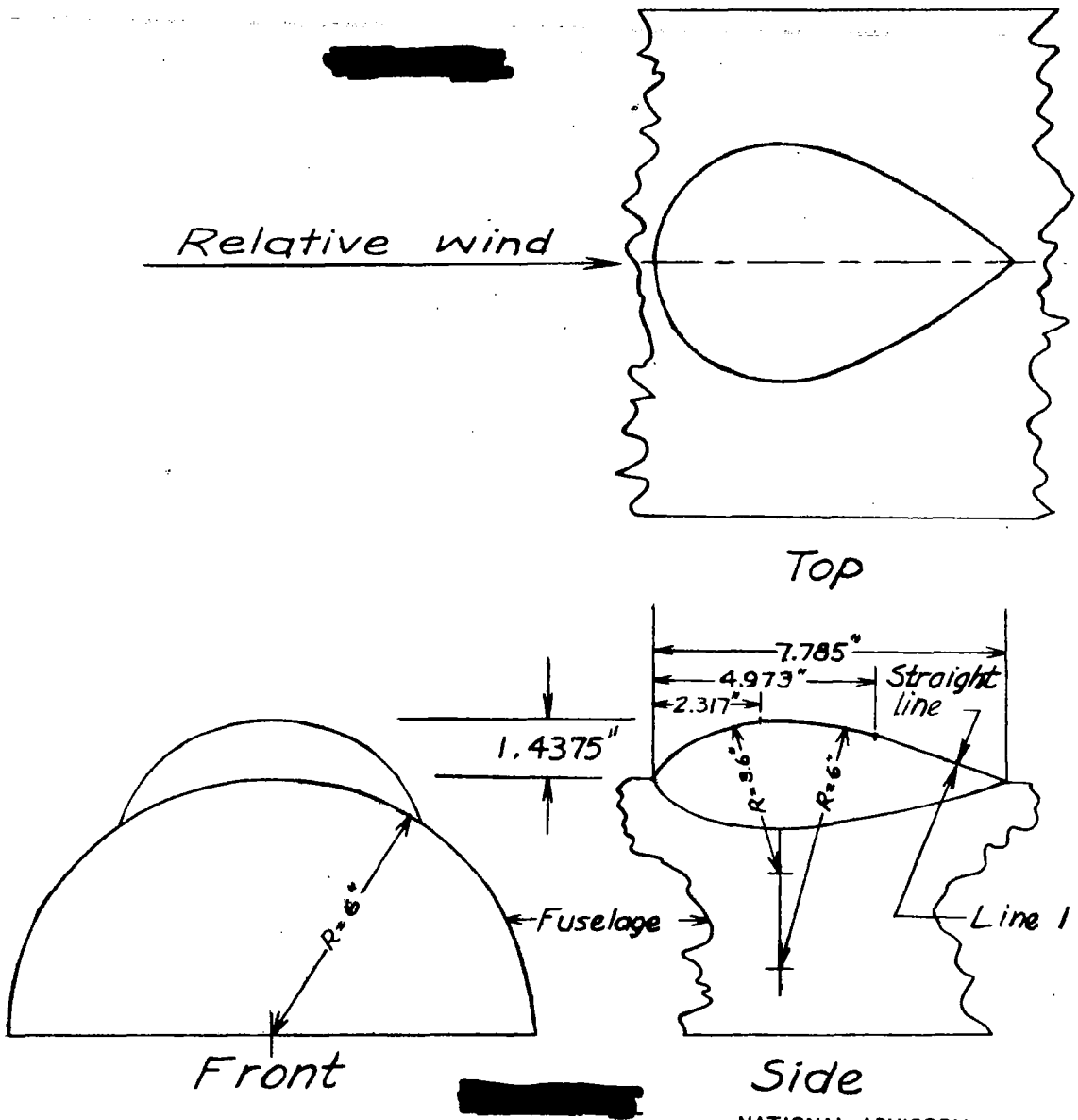

Figure 15.- Turret B details.

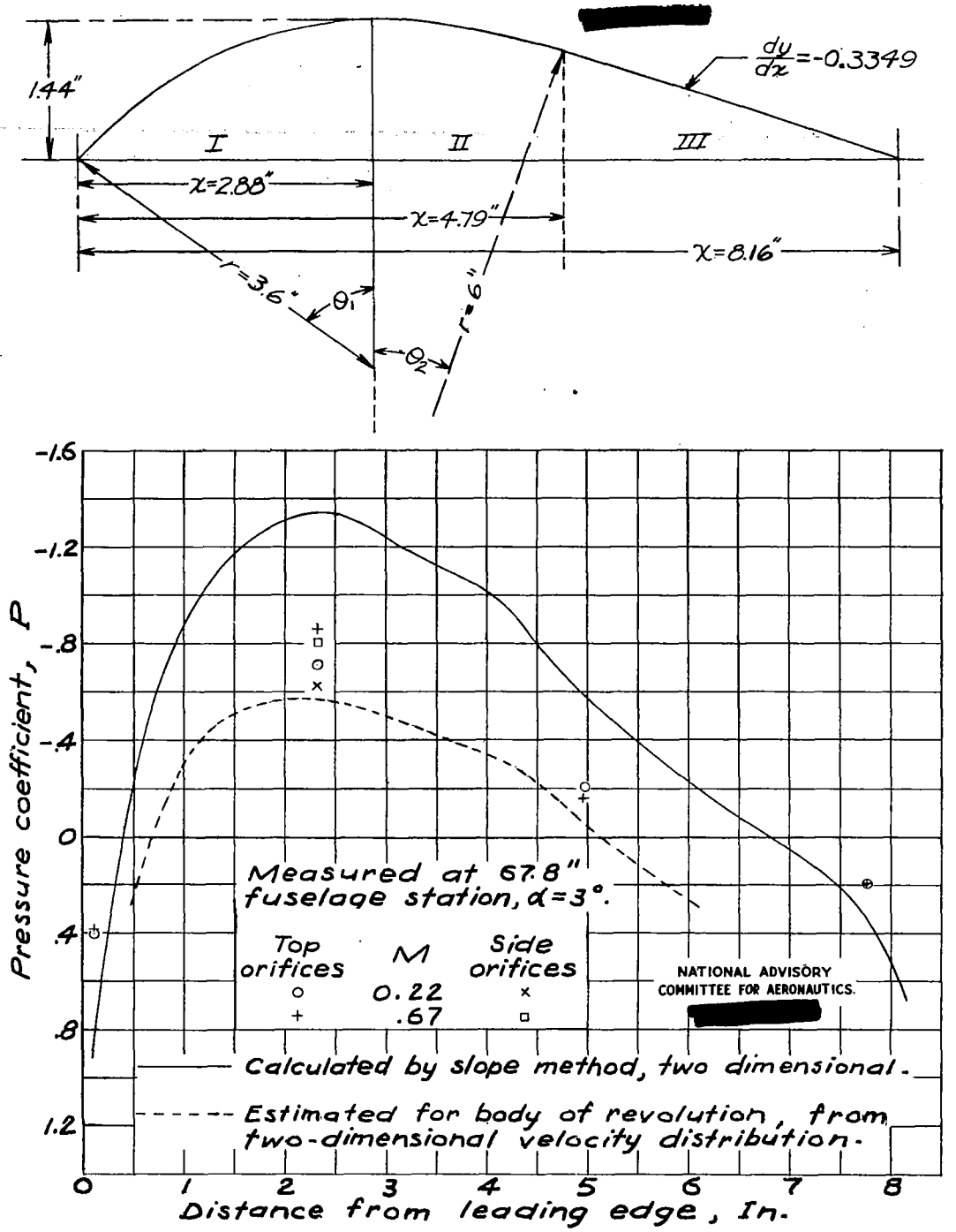

Figure 16.- Comparison of estimated with measured pressures over turret B of reference 16.

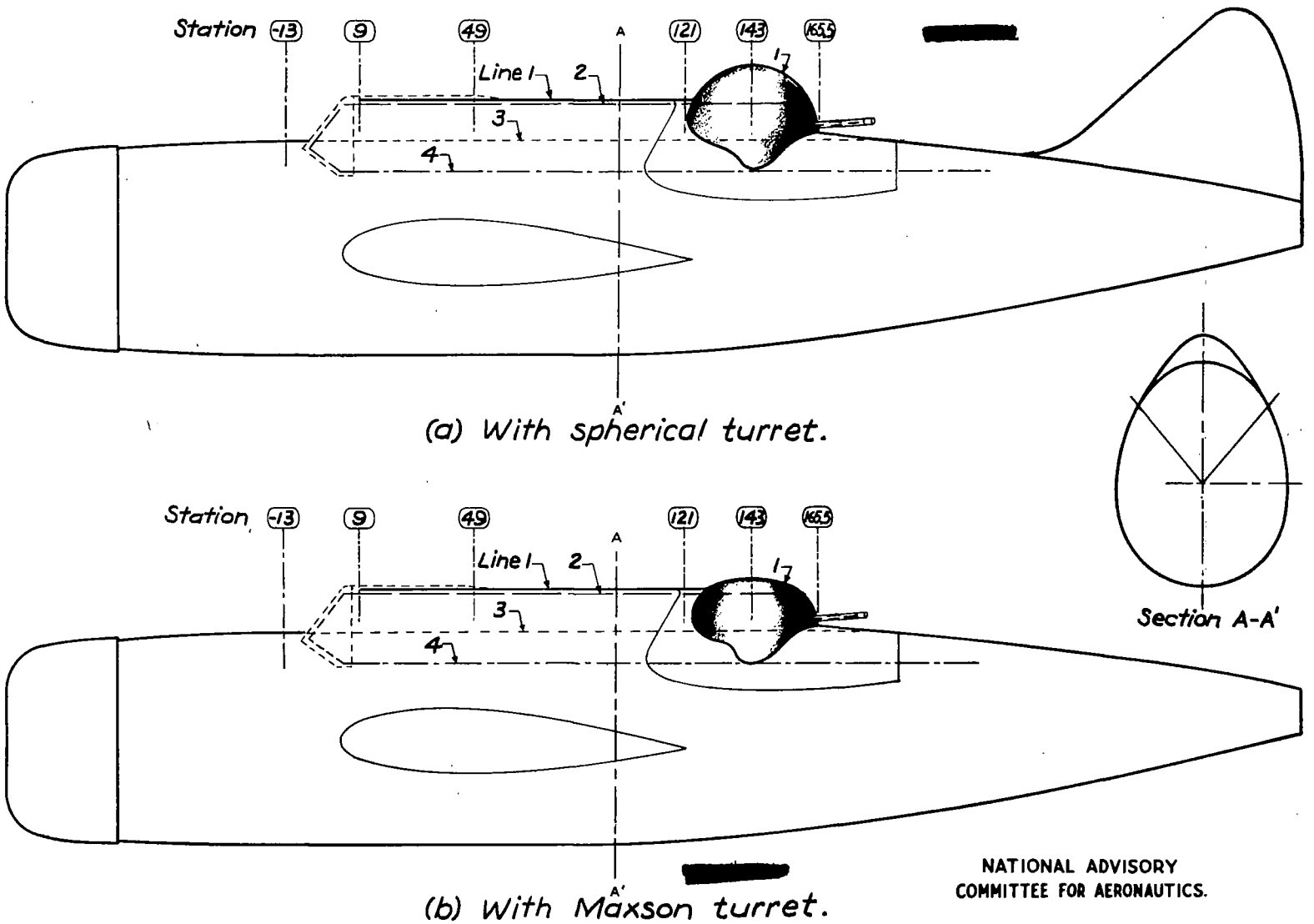

(a) With spherical turret.

(b) With Maxson turret.

Figure 17.- Locations of cockpit canopy and gun turrets on the Brewster SB-2A-1 airplane.

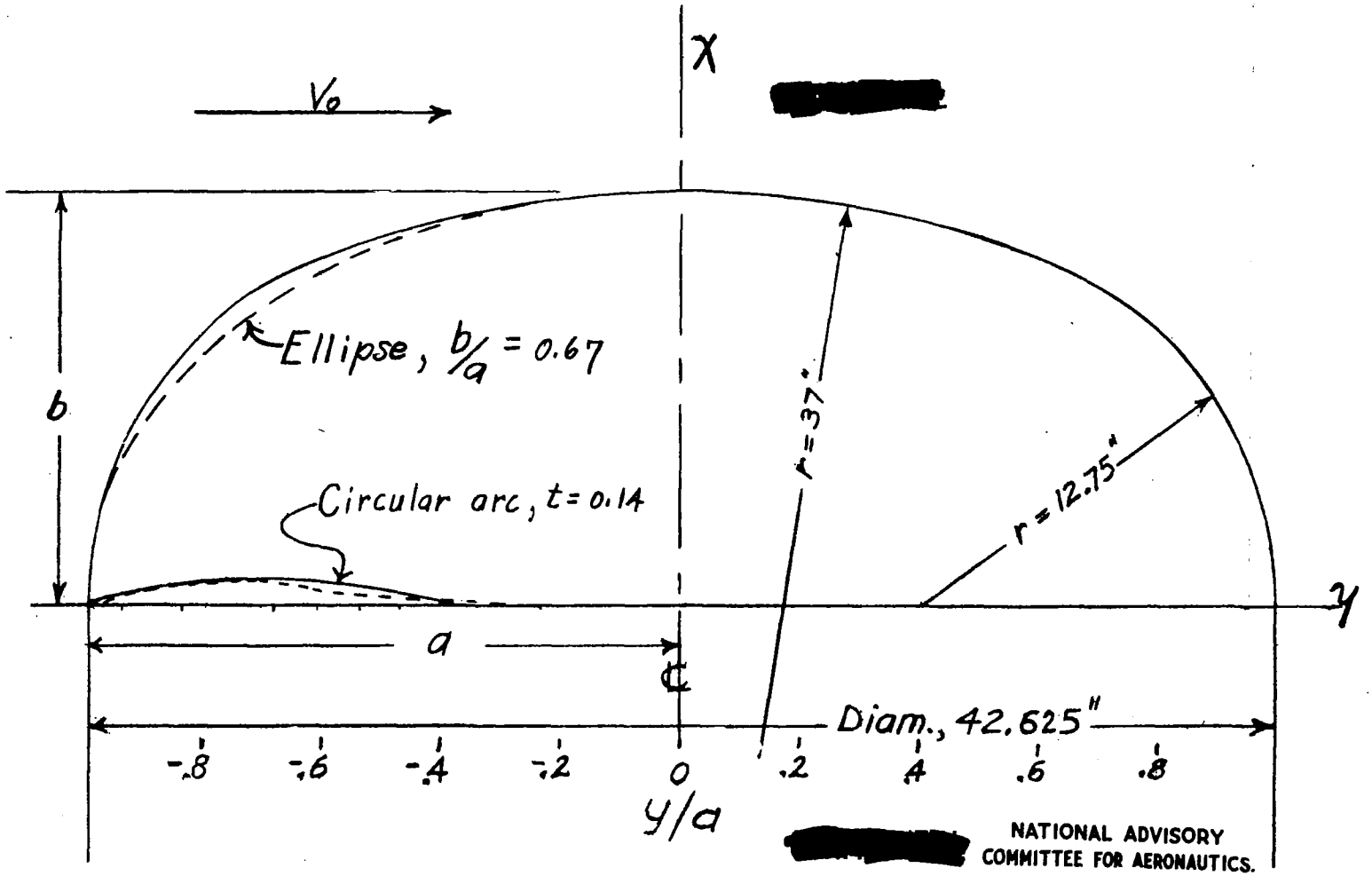

Figure 18.- Maxson gun turret; meridian profile.

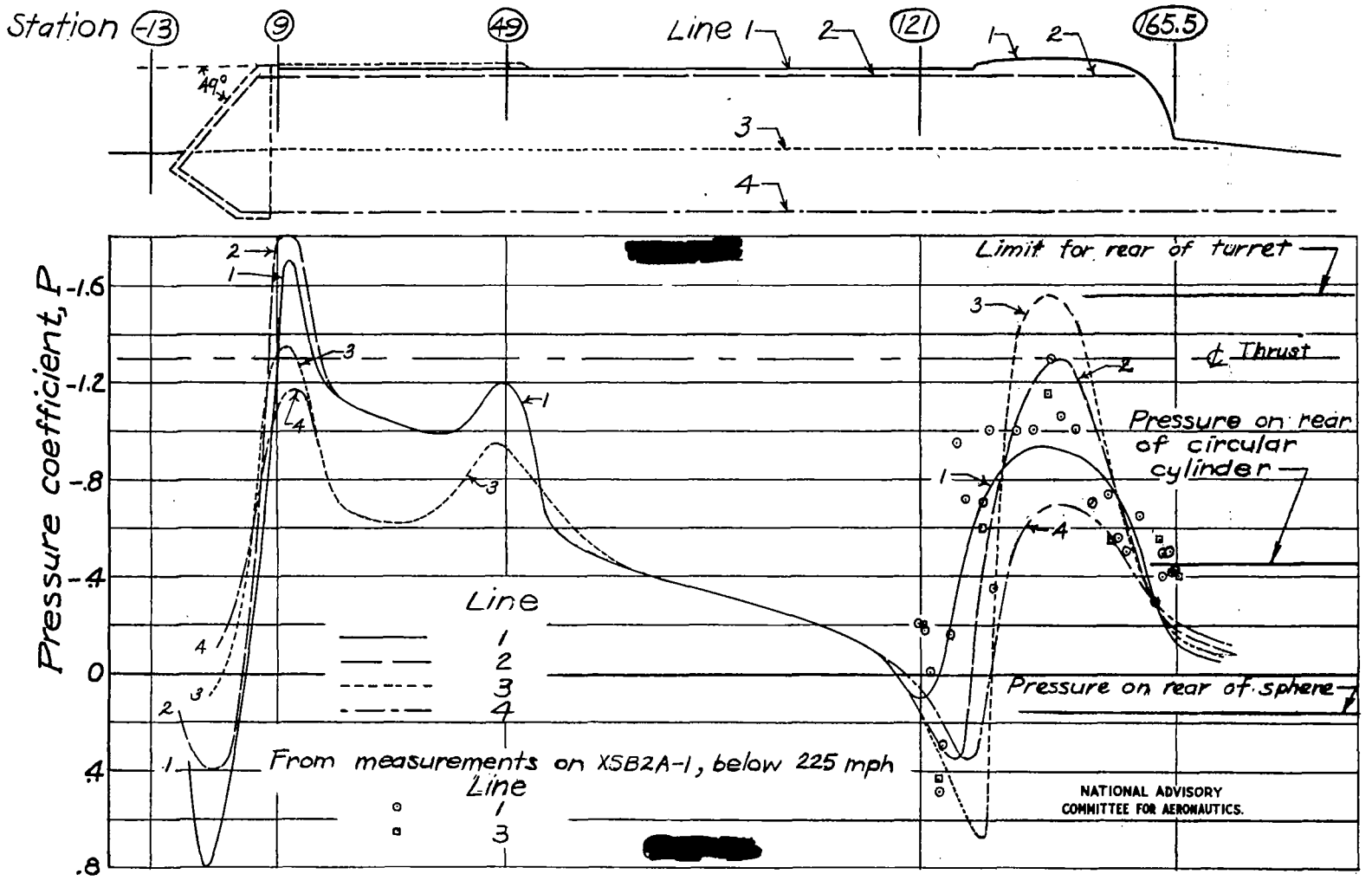

Figure 19.— Estimated pressure distribution over cockpit canopy and Maxson gun turret of Brewster SB2A-1 airplane. $M \approx 0.70$.

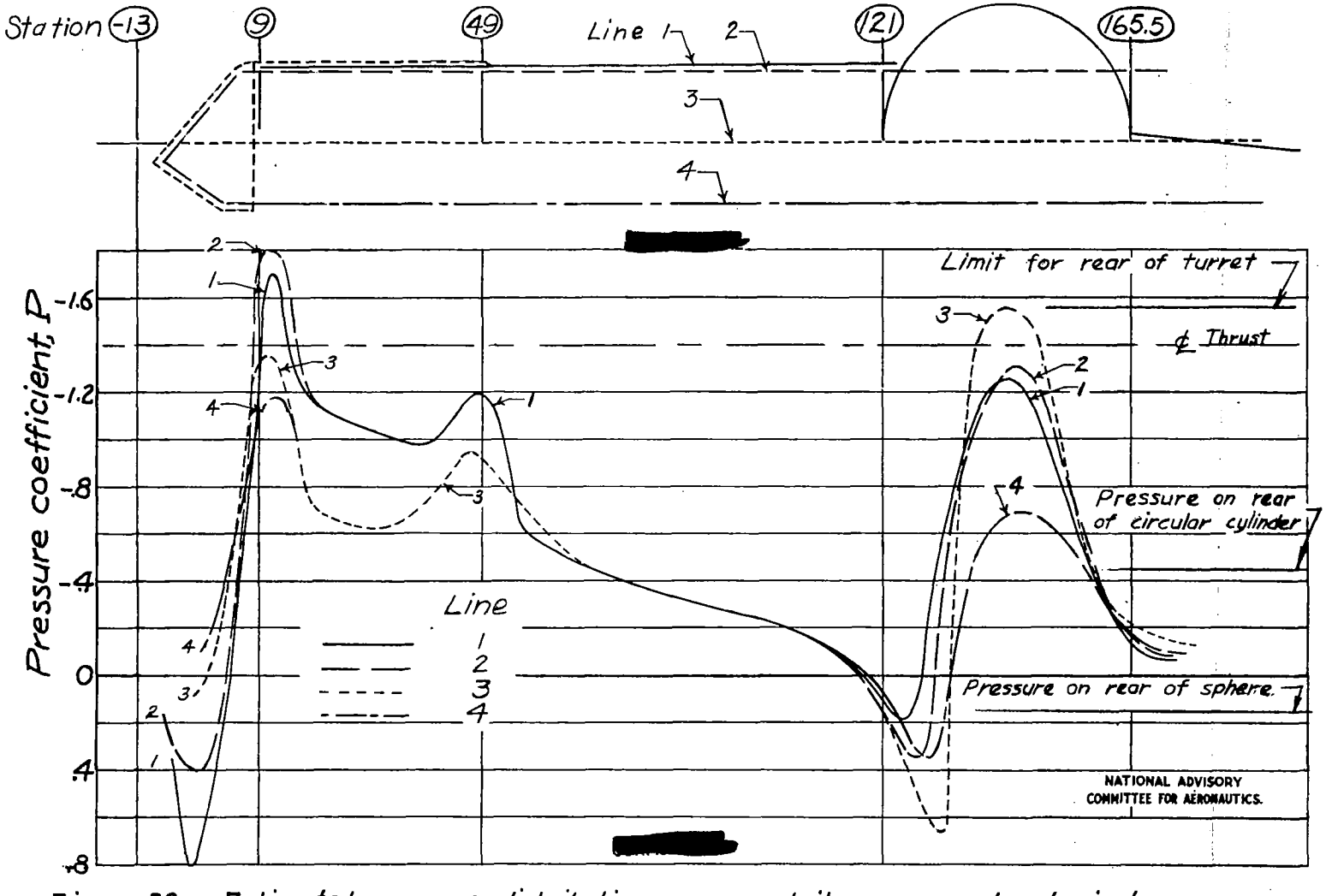

Figure 20.— Estimated pressure distribution over cockpit canopy and spherical gun turret of Brewster SB2A-1 airplane; $M \approx 0.70$.

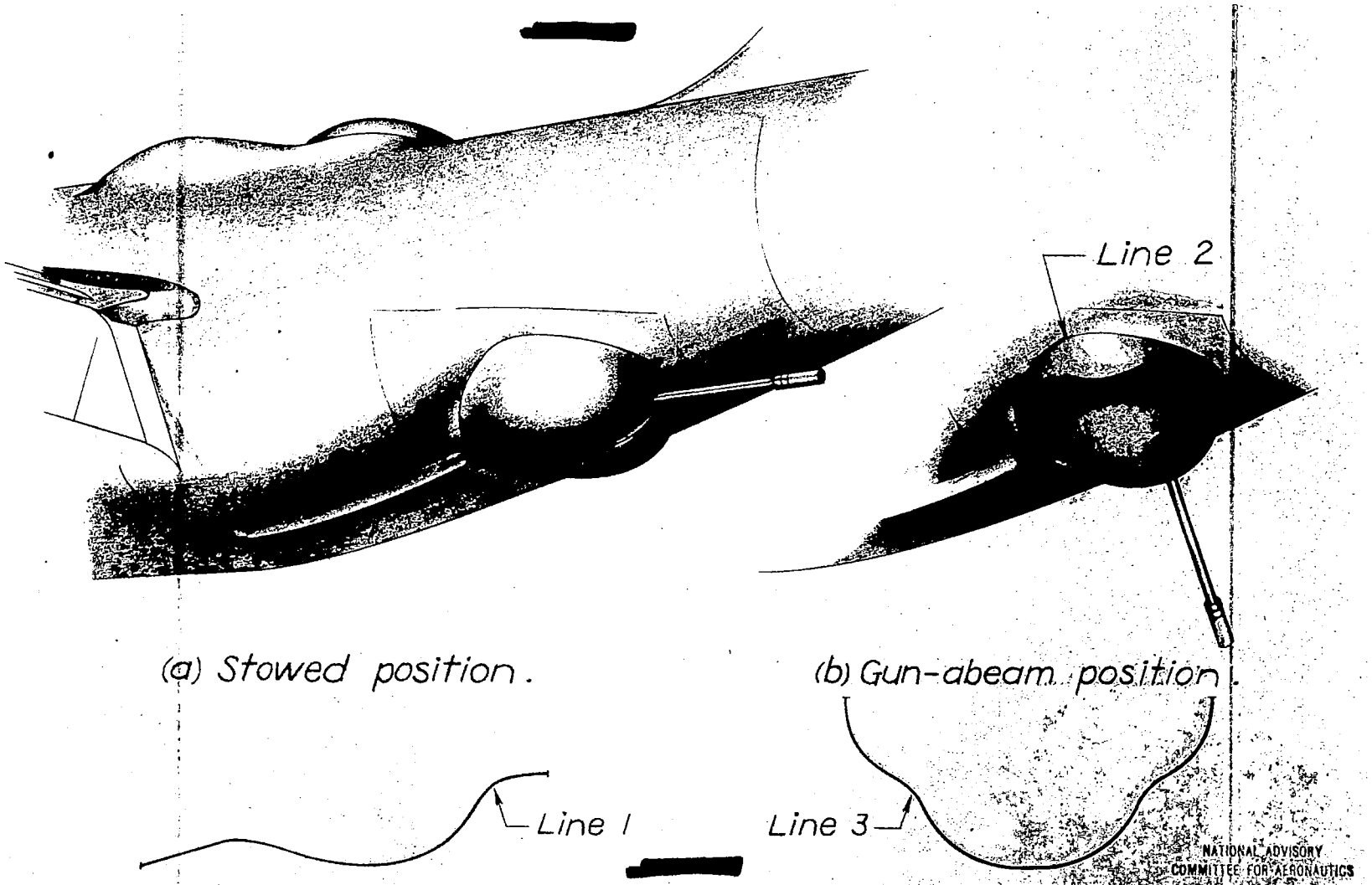

Figure 21.– Lower gun turret on Douglas XSB-2D-1 airplane.

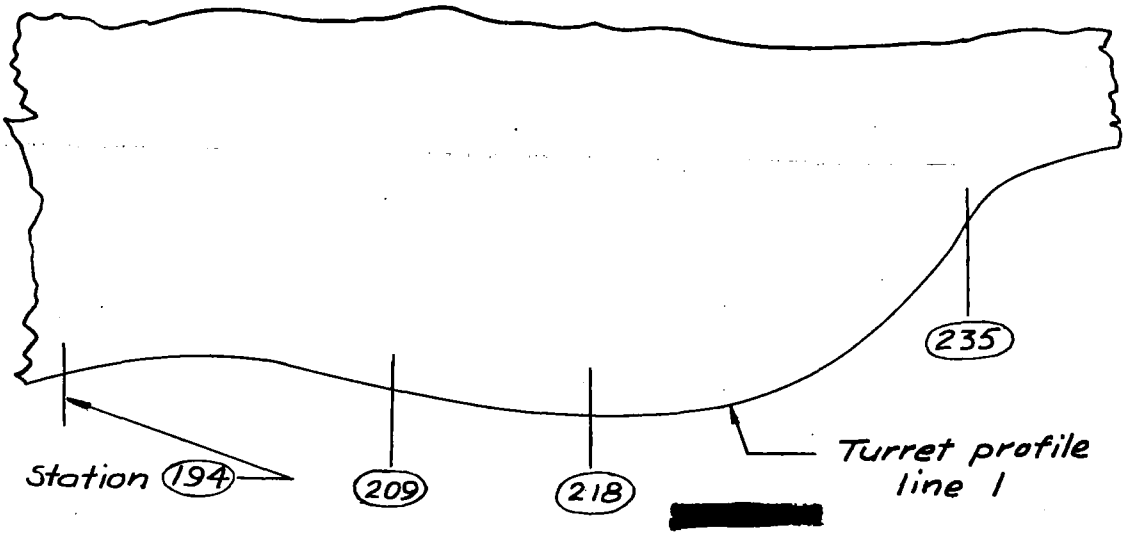

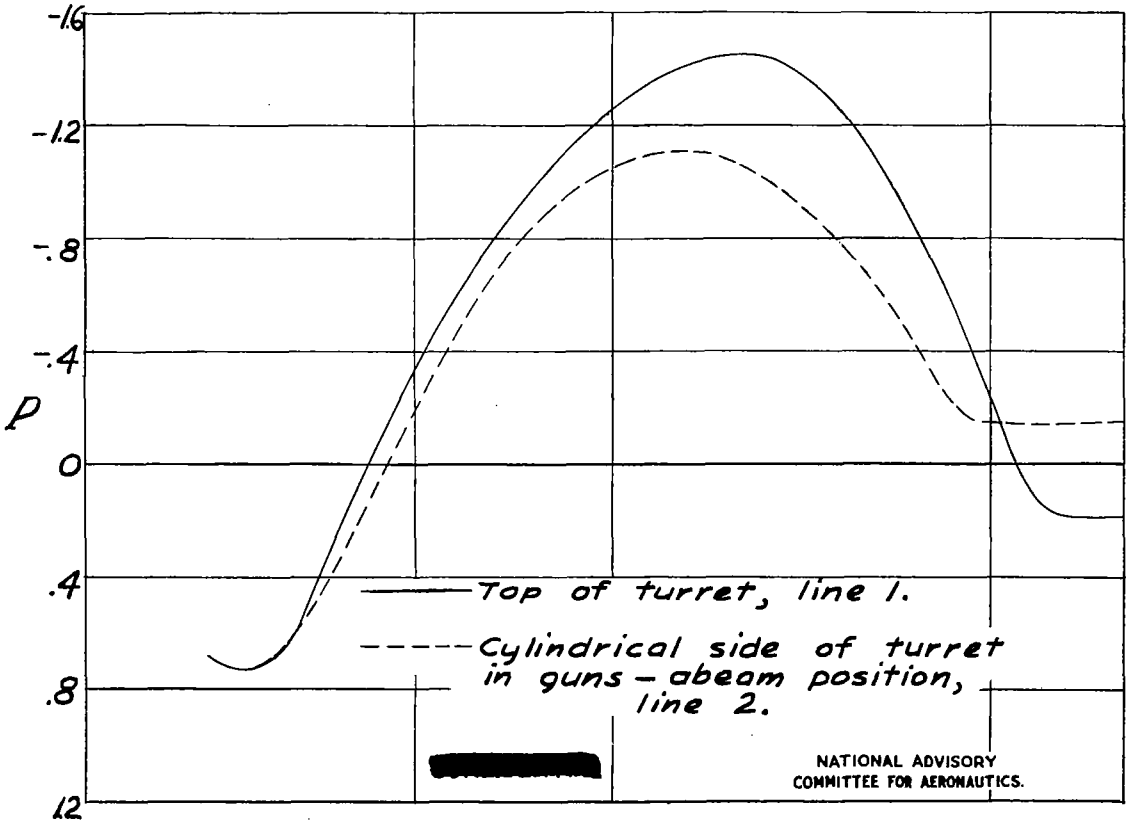

Figure 22.- Estimated pressure distribution about lower gun turret of Douglas XSB-2D-1 airplane. $M \approx 0.70$.

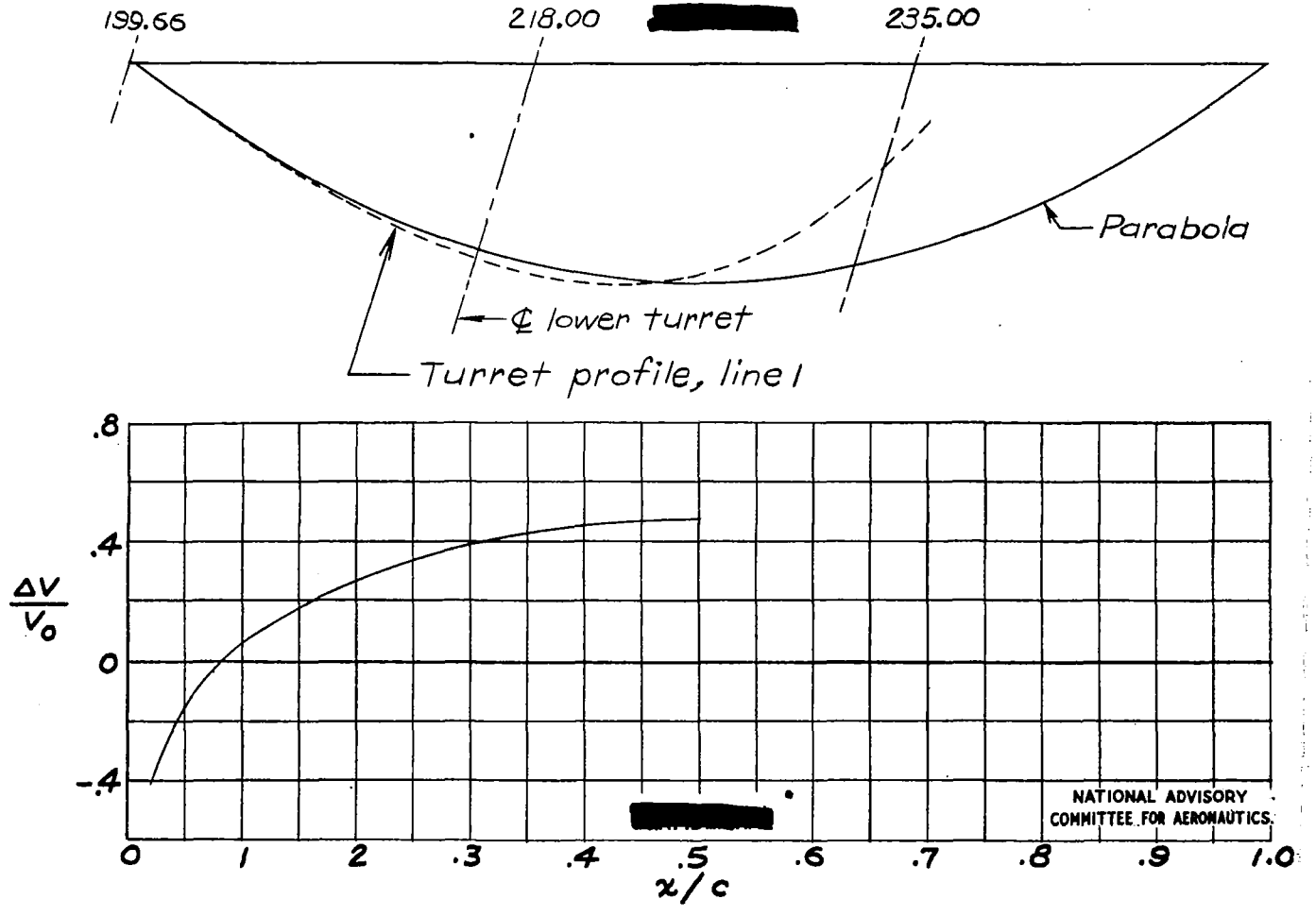

Figure 23.- Approximation of front part of lower-gun-turret profile by parabola $\frac{y}{c} = 0.744 \frac{x}{c}\left(1 - \frac{x}{c}\right)$, with velocity distribution calculated by slope method.

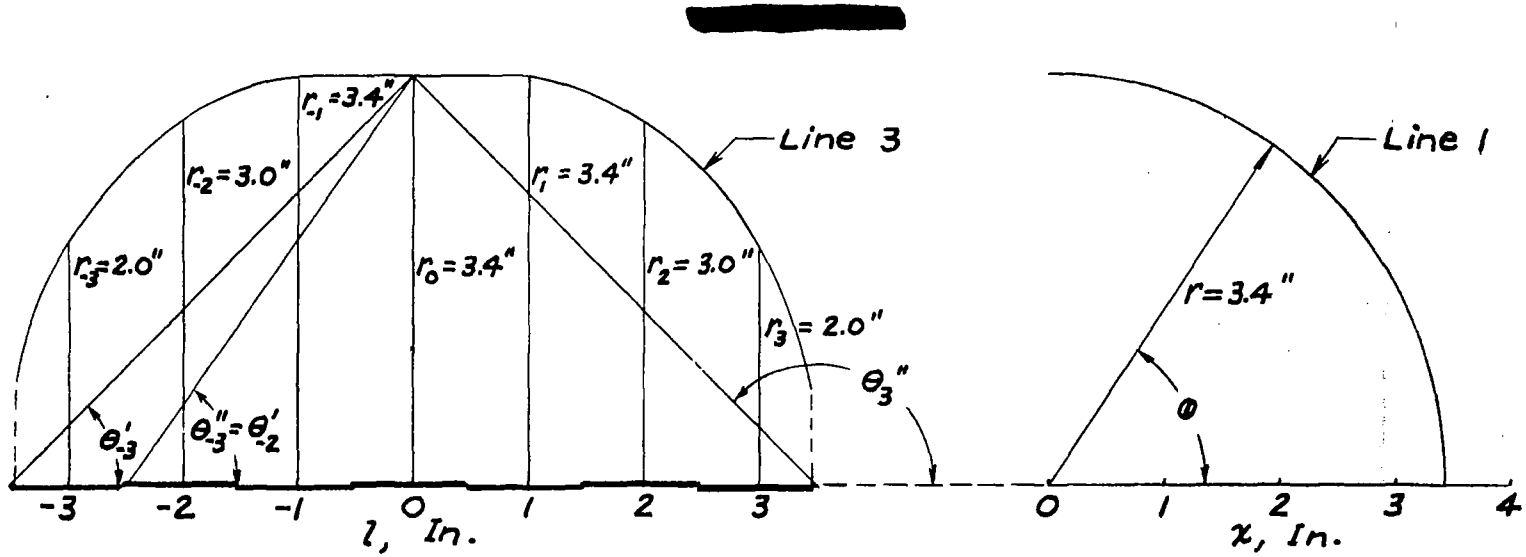

(a) Front view showing approximate cross section of turret normal to stream.

(b) Side view showing approximate profile over center in plane with stream direction.

NATIONAL ADVISORY
COMMITTEE FOR AERONAUTICS.

Figure 24.- Approximation of rear portion of lower gun turret by method of distribution of doublets along polar axis normal to stream.

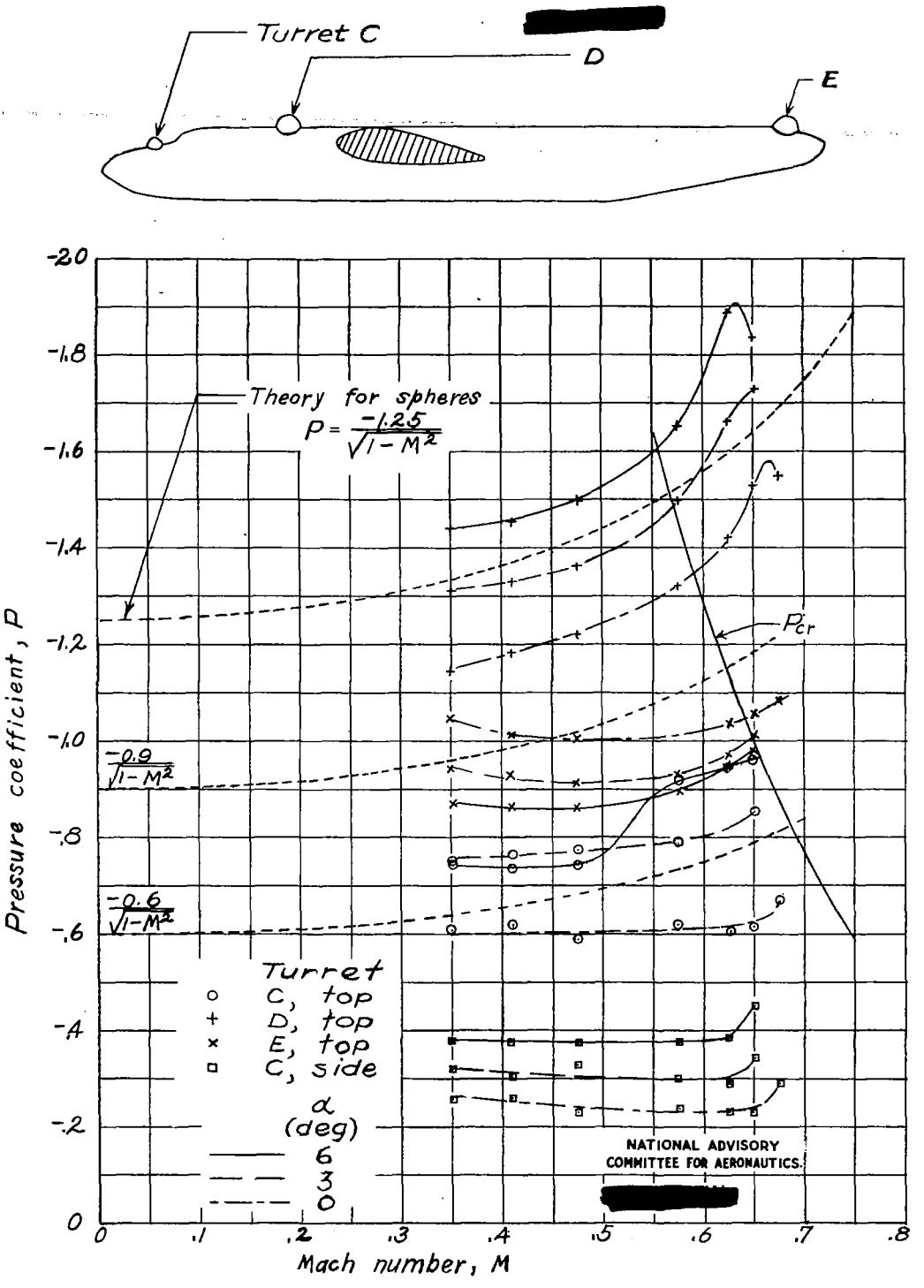

Figure 25.- Pressures on similar gun turrets in different locations on the fuselage.

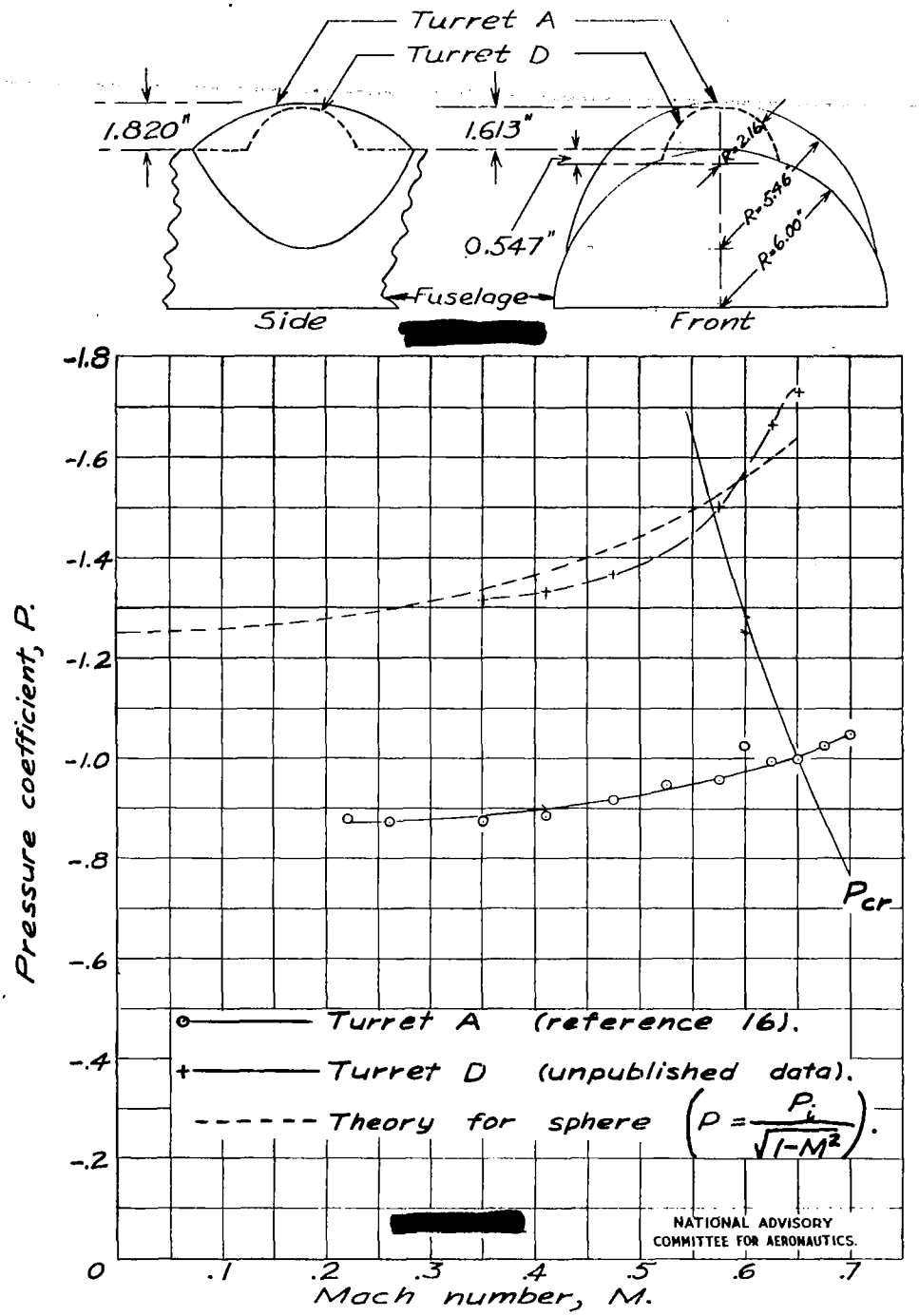

Figure 26.- Pressures on top of two spherical turrets showing effect of relative projection above the fuselage. Both turrets located at 24.9 percent fuselage length from nose. $\alpha = 3°$.

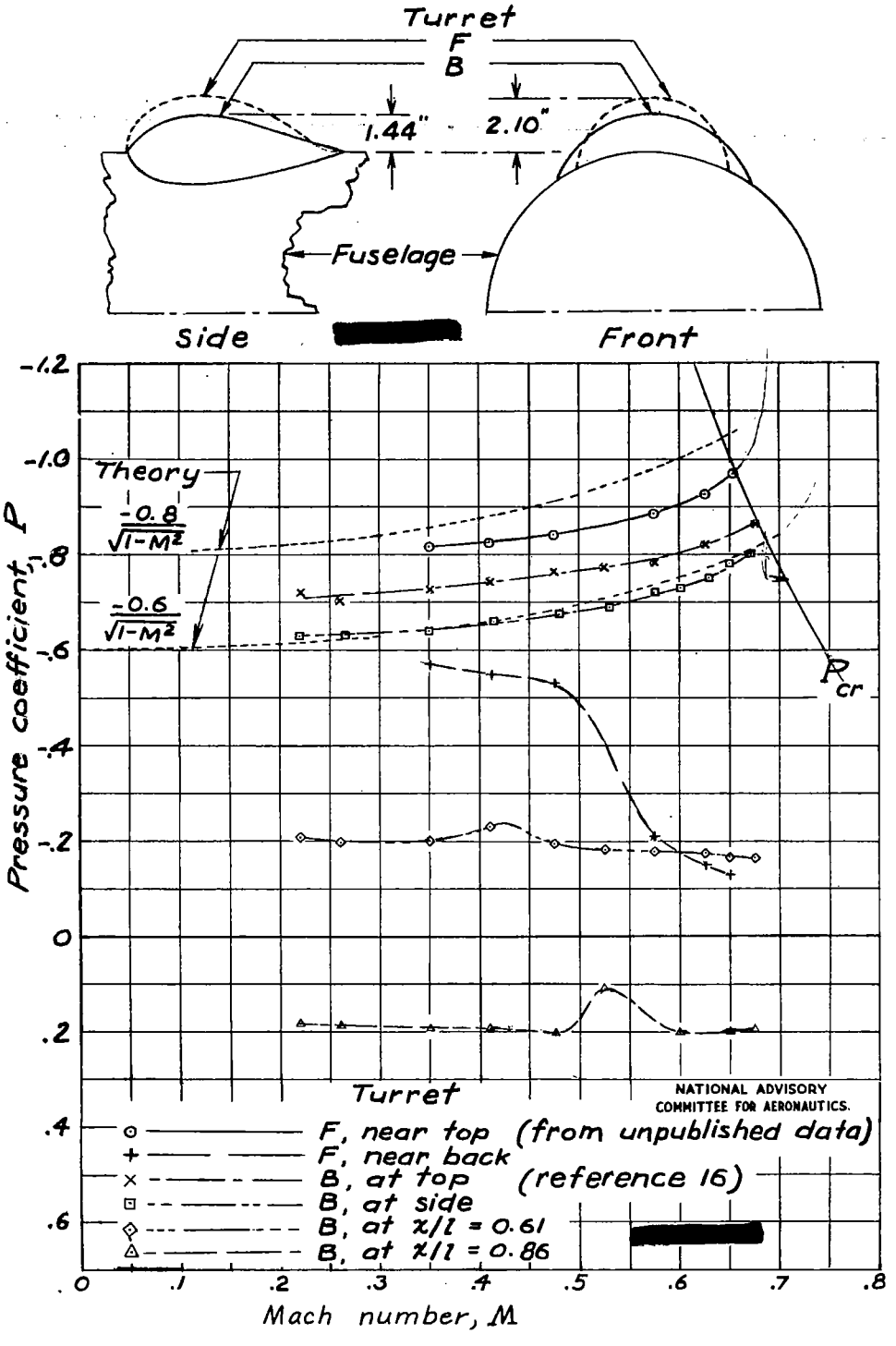

Figure 27.- Comparison of pressures on two streamline turrets of different thickness ratio showing different compressibility effects.

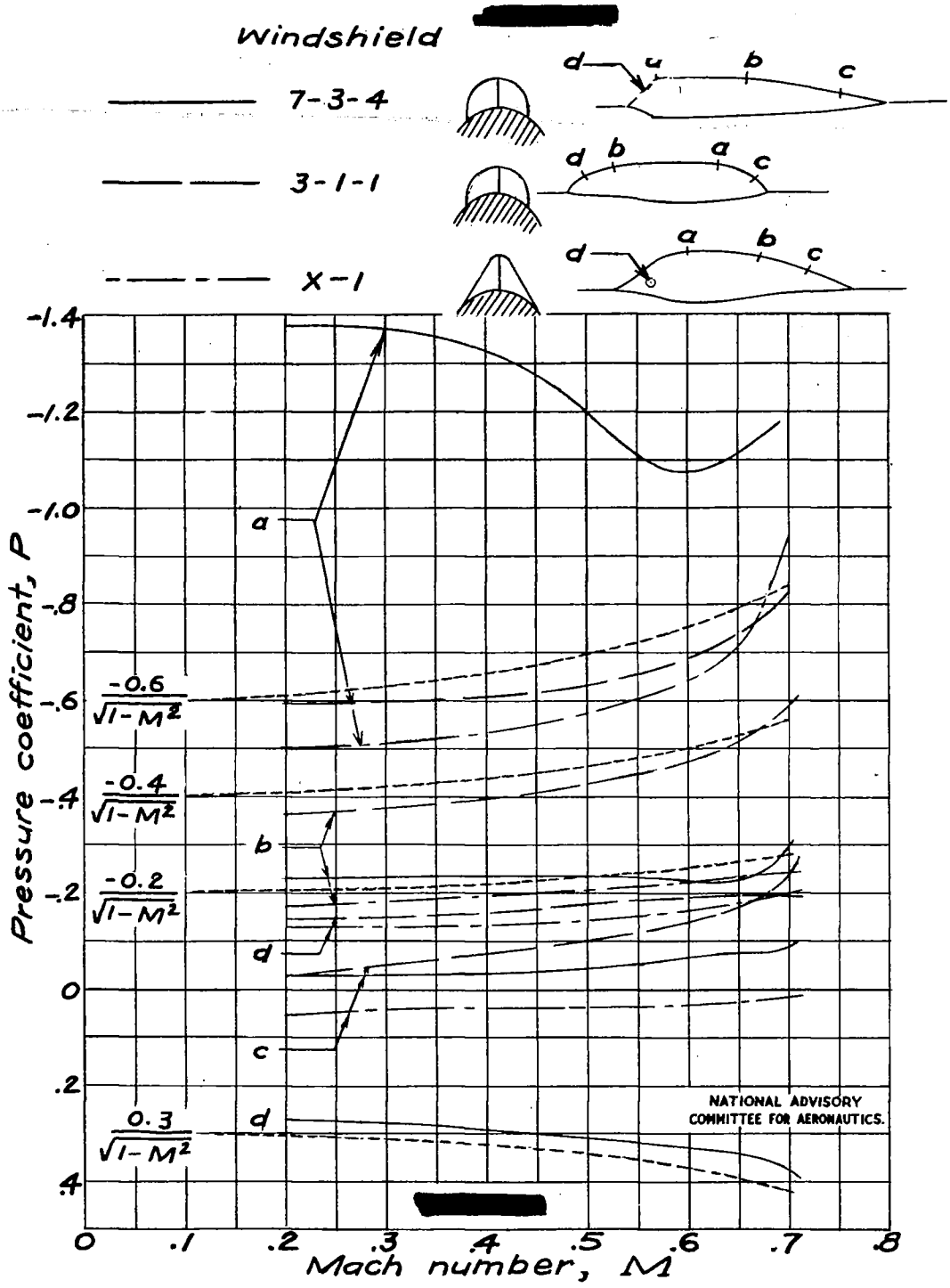

Figure 28.- Pressure change with Mach number at points on three windshields from reference 1. Point locations and corresponding pressures are indicated by the letters a, b, c and d.

TITLE: Esilmaiion of Pressures on Cockpli Canopies, Gun Turrets, Biisiers, and Similar Proiuberances

AUTHOR(S): Wrighi, Ray H.

ORIGINATING AGENCY: National Advisory Committee for Aeronautics, Washington, D. C.

PUBLISHED BY:

ATI- 7831

REVISION: none

ORIG. AGENCY NO.: ACR-L4E10

PUBLISHING AGENCY NO.:

DATE	DOC. CLASS.	COUNTRY	LANGUAGE	PAGES	ILLUSTRATIONS
May'44	Unciass.	U. S.	Eng.	79	diagrs, graphs

ABSTRACT:

Methods for esiimating pressure distribution over protuberances are described and applied to esiimation of pressure disiributions over spherical segmeni, faired gun turrets, and over proiuberances on Brewster SB2A-1 airplane. Effecis of compressibility, inierference and flow separaiion are discussed. By combining experimental data wiih theoreiical methods, limiting pressures for use in deiermining maximum ioads can be saiisfaciorily estimaied in many cases. Sysiemaiic experimentation is recommended, however, to improve accuracy of estimation.

DISTRIBUTION: Requesi copies of this report only from Originating Agency

DIVISION: Aerodynamics (2)

SECTION: Parasiiic Components and Inierference (7)

ATI SHEET NO.: R-2-7-22

SUBJECT HEADINGS: Drag, Aerodynamic - Protuberances (31250); Pressure - Measuremeni (73564)

Air Documents Division, Intelligence Department
Air Materiel Command

AIR TECHNICAL INDEX

Wright-Patterson Air Force Base
Dayton, Ohio